Morphodynamics of two Mediterranean microtidal beaches presenting permanent megacusps under the influence of waves and strong offshore winds

Pierre Feyssat, Raphaël Certain, Nicolas Robin, Jean-Paul Barusseau, Antoine Lamy, Olivier Raynal, Bertil Hebert

Morphodynamics of two Mediterranean microtidal beaches presenting permanent megacusps under the influence of waves and strong offshore winds

Pierre FEYSSAT[1], Raphaël CERTAIN[1], Nicolas ROBIN[1], Jean-Paul BARUSSEAU[1], Antoine LAMY[1],Olivier RAYNAL[1] and Bertil HEBERT[1]

1. CEFREM, UMR 5110, Université de Perpignan Via Domitia, 52 Avenue Paul Alduy, 66000 Perpignan, France. *pierre.feyssat@univ-perp.fr*

Highlights:

A conceptual morphodynamic model for two Mediterranean emerged beaches is proposed.

Offshore wind induces erosion on the backshore and produces shoreline advancement.

Beach evolutions are controlled by the balance of storms and offshore wind periods.

Fair-weather morphologies on the beachface are fully expressed due to low tidal range.

Slight differences exist depending on whether the beach is backed or not by a dune.

Abstract:

This study focuses on four years of survey of two low-microtidal emerged beaches (average tidal range ≈ 0.3 m), presenting permanent megacusps on the French Mediterranean coast. These beaches are representative of the southern part of the Gulf of Lion (45 km of coast): the Leucate beach backed by a small dune and the La Franqui beach backed by a small lagoon. An analysis of the hydrodynamic and meteorological forcing along with morphological changes allows to define the key parameters controlling the system. These results are used to develop a conceptual model composed of five main situations and then compare it to the microtidal literature. Dominant offshore winds can reach speeds of up to 20 $m.s^{-1}$ (Gusts up to 30 $m.s^{-1}$) and have an erosive action on the backshore and produce advance of the shoreline of a few metres. This shoreline advance is mainly concentrated on the horns when it is concomitant with small fair-weather waves. Waves of moderate to high intensity (storms) lead to strong erosion and steepening of the beach face, as well as the migration or

construction of a new higher berm located landward and associated with sediment deposition on the upper beach. The low tidal range may also allow the high run-up level to stabilise for a longer period of time in a high elevation on the backshore. The alternation of storm episodes and offshore wind periods could control the relative stability of the emerged beach.

Keywords: Sandy beach, Barrier beach, Emerged beach, Offshore wind, Gulf of Lions

1. Introduction

Knowledge of beach dynamics in various and contrasting environments is essential to effectively adapt management strategies and improve assessments of their resilience (Fanini et al., 2020; Power et al., 2021). Beaches are known to evolve according to forcing conditions, and this close relationship induces a cyclicity closely associated with the seasonality of weather patterns. For temperate climates, winter periods are characterised by high-energy conditions that induce erosion, while calmer summer periods allow the reconstruction of the system (Castelle et al., 2015; Konstantinou et al., 2021; Masselink and Pattiaratchi, 2001; Senechal and Ruiz de Alegria-Arzaburu, 2020). Beaches can be classified according to their morphological characteristics. One of the most widely used classifications of beaches is based on the Australian model, which is drawn from the study of sandy beaches along a microtidal coastline with moderate to high wave energy and is mainly focused on the dynamics of nearshore bars (Wright and Short, 1984). This study has since been extensively applied to other environments, but always remaining focused on the dynamics of nearshore bars and little on the morphodynamics of the emerged beach (Aleman et al., 2015; Castelle et al., 2007; Lippmann and Holman, 1990; Masselink and Short, 1993; Scott et al., 2011). The model assumes that a system can evolve towards a dynamic steady state under stable forcing conditions. Thus, several main beach states are recognized: reflective, intermediate and dissipative. Intermediate beaches can display large-scale rhythmic crescentic features along the shoreline called megacusps. These megacusps are usually defined as a succession of horns extending seaward and embayments extending landward (Thornton et al., 2007). The patterns of horns and embayments are induced by hydrometeorological forcing and antecedent morphology (Benavente et al., 2011; Coco et al., 2000; Guza and Inman, 1975). The beach is narrower and lower in the embayment of the mega-cusps, which allows the swash of large storm waves to reach a maximum elevation on the beach (e.g. Castelle et al., 2015; Short and Hesp, 1982; Thornton et al., 2007; Wright and Short, 1984). The response of

these features is however complex and needs further investigation, although some studies have found that megacusps are forming during less energetic condition and disappearing during storms (Birrien et al., 2013), others have also observed megacusps persisting during storms (Aagaard et al., 2005; Castelle et al., 2019; Quartel, 2009) and disappearing during less energetic wave conditions (Segura et al., 2018).

As previously stated, most researches had focused primarily on coastline and nearshore morphodynamics, but the study of emerged beach (backshore) dynamics, which is the part of the beach between the beach face and the dune foot is particularly relevant since it addresses many scientific concerns (Eichentopf et al., 2019a; Fanini et al., 2020) and socioeconomic issues (Fanini et al., 2020). Most of the studies on emerged beaches refer to moderate to high-energy and/or meso to macrotidal coasts. Only limited research has been undertaken for example on emerged beaches subject to long period of fair-weather interspersed with short and energetic storm event intermittent forçing (like the intermittent forcing of the Mediterranean, e.g. Amores et al., 2020; Buosi et al., 2019; Gervais et al., 2012; Sabatier et al., 2008) or low energy, which have been shown to respond very differently to changing wave conditions (Costas et al., 2005; Gómez-Pujol et al., 2007; Hegge et al., 1996; Jackson et al., 2002). Moreover, in microtidal environments, attention has been mainly given to storm effects and beach recovery processes (Davidson et al., 2013; Eichentopf et al., 2020; Gallop et al., 2011; Phillips et al., 2017) as well as shoreline dynamics (Davidson et al., 2017; Van Gaalen et al., 2011; Yates et al., 2009), inlet dynamics (Kennedy et al., 2020; McSweeney et al., 2020; Meslard et al., 2022), aeolian processes (Lynch et al., 2013; Schwarz et al., 2021) or beach-dune interaction (Medellín and Torres-Freyermuth, 2021; Short and Hesp, 1982; Thornton et al., 2007). These studies are mainly concentrated on sites where the tidal range is close to the upper class limit (2 m) and the impact of certain processes is not fully investigated. This applies to aeolian processes, which can give rise to considerable sediment transport and significant morphological evolution on the backshore (Bauer et al., 2012; Gares et al., 1996; Nordstrom et al., 1996; Nordstrom and Jackson, 2017), or the impact of long periods of fair-weather (Buosi et al., 2019; Gómez-Pujol et al., 2011; Longhitano, 2015). Environments with a low tidal variation (Tidal Range < 0.5 m) are common in large lakes (Law and Davidson-Arnott, 1990a) or enclosed basins such as the Azof, Baltic (Käärd et al., 2016; Soomere et al., 2020), the Mediterranean or the Black Seas. In these environments, wave energy is primarily distributed at the same elevation due to the low tidal range (Cooper, 1994) inducing a time action of hydrodynamic processes different from higher tidal environments. The northwestern Mediterranean is an example of a singular low microtidal

environment with a very narrow intertidal zone (less than a few meters). This area is also characterized by long fair-weather periods of weak wave energy interspersed with short high-energy storms (Aleman et al., 2015; de Swart et al., 2022) where the significant wave height (Hs) can reach 6 m, inducing a surge level close to 1-1.5m (Aleman et al., 2015; Guizien, 2009; Mendoza et al., 2011). In these singular environments, the backshore is only subject to the influence of marine processes during these short storm periods (Armaroli et al., 2013, 2012; Balouin et al., 2013; Gervais et al., 2012b; Romagnoli et al., 2021; Sabatier et al., 2008; Sedrati et al., 2011). Such episodes can also lead to an impact on coastal infrastructures (De Muro et al., 2017; Porta et al., 2020; Trogu et al., 2020). Despite the fact that low-microtidal environments can be potentially affected by long fair weather periods, it should be distinguished from the low-energy environments defined by Jackson et al. (2002). These latter are commonly observed on beaches in estuaries and bays or on sheltered coasts where non-storm significant wave heights are minimal (<0.25 m) and waves are of small amplitude, despite strong onshore wind forcing (<0.50 m). During the long periods of weak waves in the northwestern Mediterranean, changes in beach-face morphology can be relatively intense (Bertoni et al., 2013; Sedrati et al., 2009) and the wind regime is also to be considered in the evolution of the system as the beach exposure time is sufficient to cause onshore and offshore transport and induce morphological changes on the backshore or the beach face (Feyssat et al., 2022; Law and Davidson-Arnott, 1990b; Sabatier et al., 2007). As a result, the coastal Mediterranean environment is complex, with processes (offshore/onshore) acting in very different ways in both time and space.

The aim of this study is to complete the conceptual beach models, using simple semi-quantitative parameters and only focusing on the emerged beach. This involves discriminating the influence of each control parameter on the emerged beach morphodynamics, with particular emphasis on fair-weather and offshore wind conditions which are less discussed in the literature. Two sandy beaches evolving in a low-microtidal environment were surveyed over four years. The methodological approach is based on frequent topographic surveys as well as hydrodynamic and meteorological data from nearby stations. The results are then summarised in a conceptual beach model that combines a set of factors (wave and wind) that are not usually considered simultaneously and compared to the microtidal literature.

2. Study area

The Gulf of Lions is a low-microtidal, wave-dominated environment with an average tidal range <0.3 m at mean spring tides. Under stormy conditions, a surge of about 1 m may occur due to the combined action of onshore wind stress, the reduction in atmospheric pressure and/or breaking waves (Certain, 2002).

Weather patterns can be divided into two main regimes as follows. The prevailing offshore winds (NW) frequently reach daily average speeds of more than 10 $m.s^{-1}$ with speed gusts exceeding 30 $m.s^{-1}$ for a few hours (**Fig. 1a**). This strong offshore wind generates waves that propagate away from the study sites (Grey area **Fig. 1b**). Onshore winds (SE) are less frequent (**Fig. 1a**) and are accompanied by waves (mean annual Hs = 0.66 m) or winter storms (Aleman et al., 2015). The S/SE swell (**Fig. 1b**) is characterised by higher wave heights and long periods ($5 \leq Ts \leq 10$ s), due to the more extensive fetch (Certain, 2002). In the present study, a storm is defined as a wave event in which Hs exceeds the 2 m threshold value commonly used in the region (Aleman et al., 2011; Mendoza and Jiménez, 2006). According to this definition, on the Leucate site, about 7 to 8 storm events are reported per year (Cerema and Dreal LR, 2018). Hs can reach up to more than 6.5 m during severe storms (Cerema and Dreal LR, 2018; Certain, 2002). A seasonality pattern can be observed: in summer, sea breezes are frequent, whereas, in late autumn, winter and spring, there are stronger offshore wind episodes interspersed with storms induced by onshore winds (Certain, 2002).

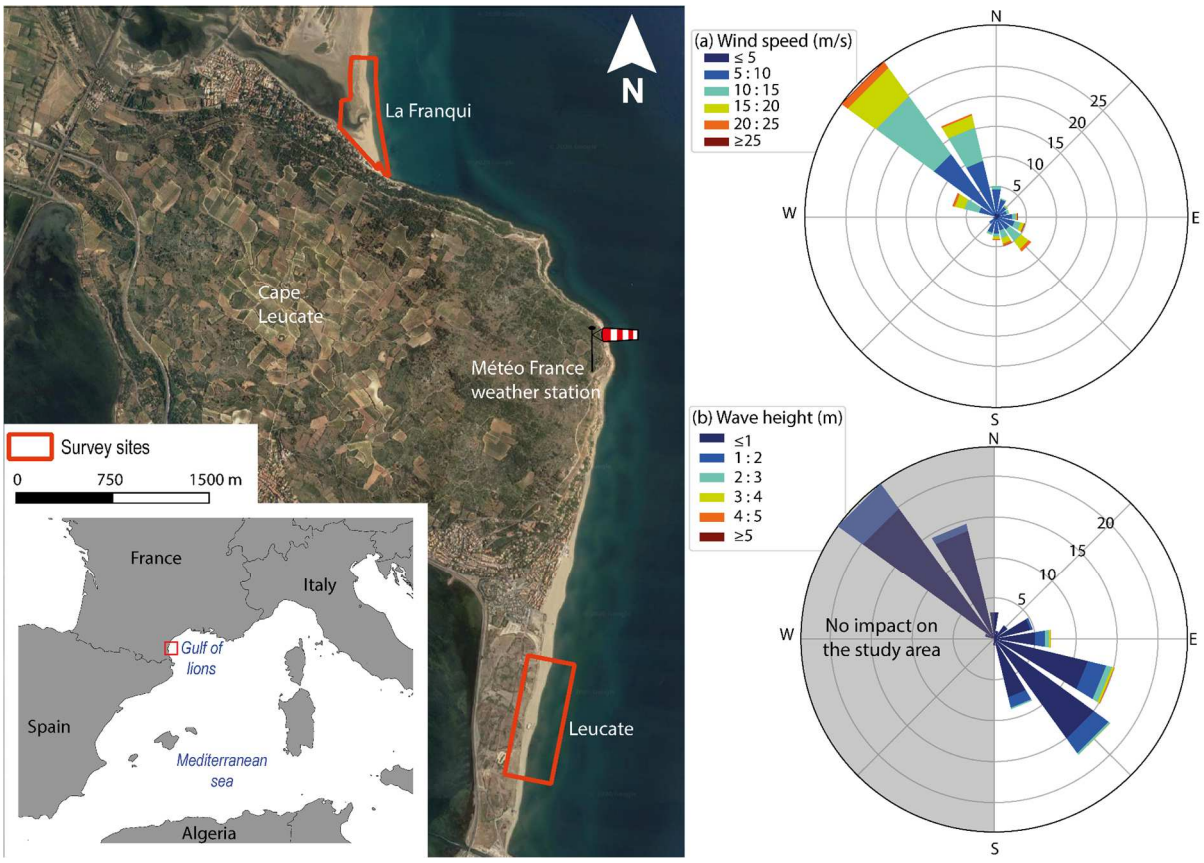

Figure 1 Location of study sites (outlined in red). (a) Wind conditions (measured at the tip of Cap Leucate). (b) Wave conditions (measured at 40 m depths, about 2.1 nautical miles in front of the weather station*). Meteorological data are given for the period 2007-2020.*

The study sites (Leucate and La Franqui) are both located in the south of the Gulf of Lions, on both sides of Cape Leucate (French Mediterranean coast) (**Fig. 1**). These two sites are representative of the beaches in this coastal area, which are described as intermediate, with a permanent double crescentic nearshore sandbar system giving an undulating pattern to the coastline (Aleman et al., 2015, 2011; Ferrer, 2010). These beaches show an alternating pattern of horns and embayments (**Fig. 2a, b**), with varying depths and a wavelength of about 80 to 100 m at La Franqui (**Fig. 2a & 3 c**) and 100 m at Leucate (**Fig. 2 b & 3 b**). These megacusps are relatively stable over time (even on an annual scale) and show very little longshore migration during a single storm, which is not common, due to the stability of the nearshore bars (Ferrer, 2010). To the south, the Leucate site (**Fig. 2 b & 3 b**) corresponds to a barrier beach made up of mostly coarse-grained sand (D50= 0.75 mm). The beach width is about 70 m and is backed by a small vegetated dune, mostly artificial and stabilised (fencing and vegetation), with a dune foot located at 2 m NGF (NGF, French national topographic reference) (**Fig. 4b**) and its elevation reaching up to 4.5 m NGF. Similar sites are shown in yellow on the map (**Fig. 3a**), representing 42% of the depicted coastline. To the north, the La

Franqui barrier beach (**Fig. 2a & 3 c**) is also mostly coarse-grained sand (D50= 0.5 mm). The beach width is about 90 m and is directly backed by a small shallow lagoon, displaying an intermittent inlet on the southern part (**Fig. 3c**). It shows a flatter profile only reaching around 1.6 m NGF, without a dune system (**Fig. 4a**). Similar sites are shown in green on the map (**Fig. 3a**), representing 26% of the depicted coastline, mainly located in the northern part. The longshore drift is oriented northward at both sites (Kulling, 2017).

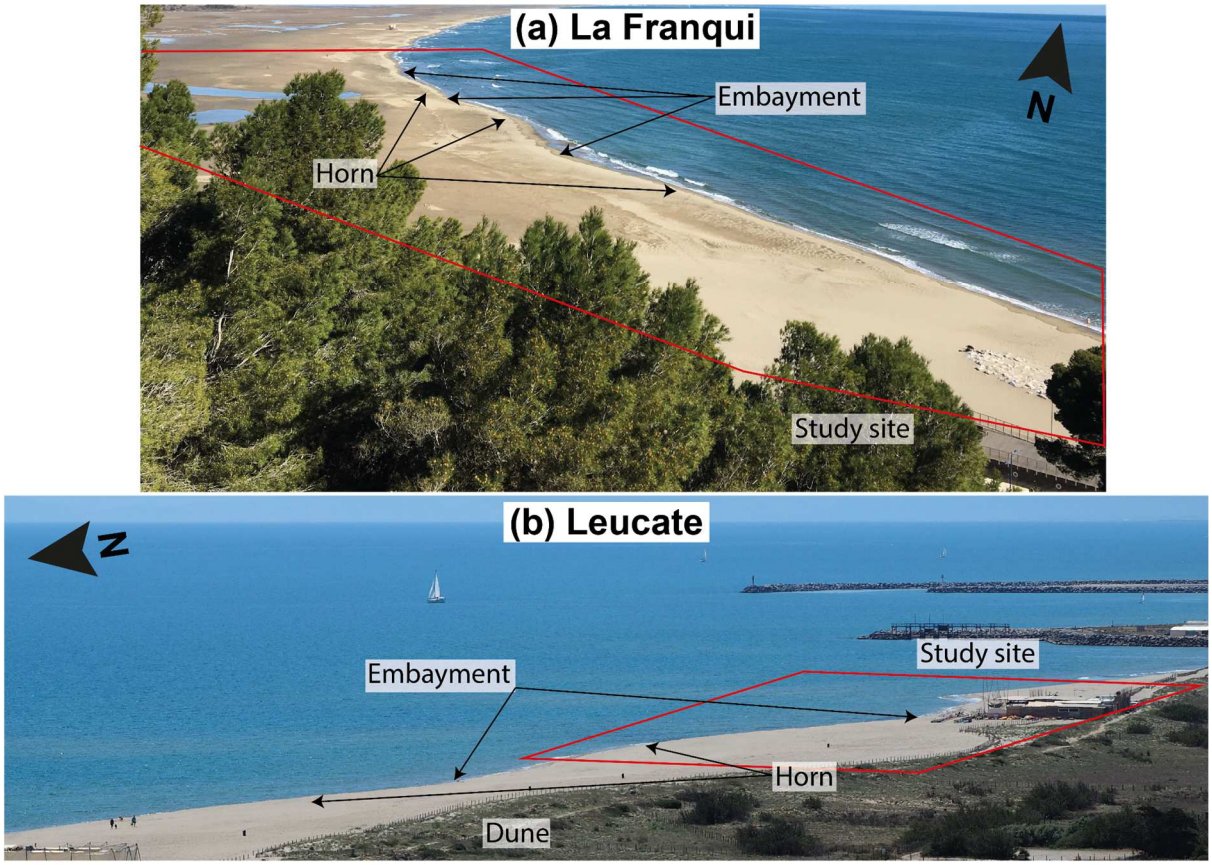

Figure 2. Oblique aerial views of the La Franqui (a) and Leucate (b) study sites with the location of horns and embayments.

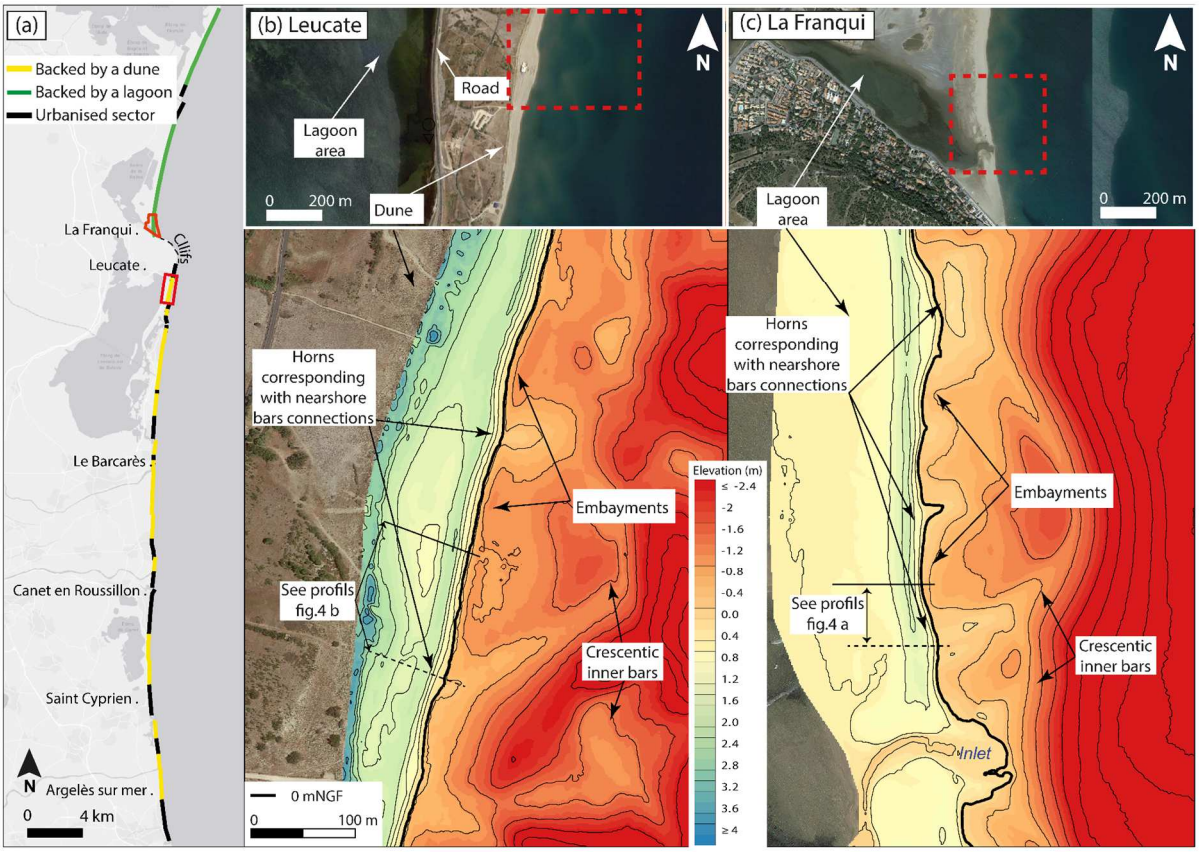

Figure 3 (a) Regional classification of beaches presenting permanent megacusps, differentiating those that are backed by a dune (yellow), not backed by a dune (green) or urbanised (black); red square corresponding to study sites. LiDAR topo-bathymetry of Leucate (b) and La Franqui (c), thick black line is 0 m NGF corresponding to the mean sea level; dashed red squares on the aerial photos correspond with the topobathymetric coverage area. See Figure 4 for beach elevation profiles.

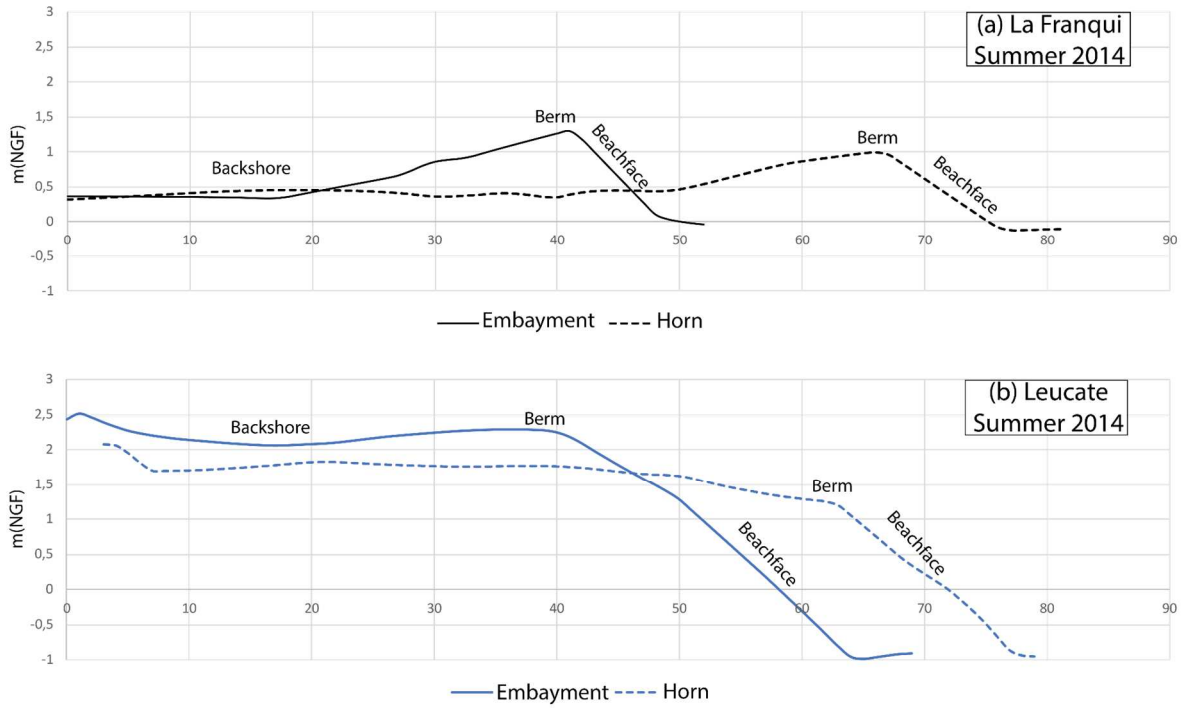

Figure 4 Topographical transects sections at the Horns (dotted lines) and embayment (solid lines); for the beach of a) La Franqui and b) Leucate. See the position of the profiles on Figure 3 b and c

3. Methods

3.1 Morphological Surveys

The beach morphological survey was carried out using a DGPS-RTK mounted on a load carrier following transverse transects spaced at 10 m and supplemented by longitudinal transects for the coastline and the berm crest. The shoreline is defined as the static position of the water body on the field by the operator for this no-tidal environment, and the berm crest is defined as the highest point of the berm. Surveys were performed using an Ashtech Proflex 500 and a Trimble R8s. Digital elevation models (DEM) were generated on QGIS using the natural neighbour interpolation method (cell size : 0.5m, Z precision ≈ 2.5 cm). Using benchmarks located on the beach, the operational accuracy of individual surveys was estimated at +/- 3.5 cm including instrument, field measurement and interpolation uncertainties. Thus resulting in a +/- 5 cm uncertainty margin on differentials between two surveys. The survey is event-based, with measurements taken before and after morphogenetic periods. A total of 44 DEMs were generated and used for this study over a survey period ranging mostly from November 2017 to May 2019 for the La Franqui beach and from July 2019 to December 2020 for the Leucate beach (**Fig. 5**).

3.2 Hydrodynamic and meteorological data

Offshore wave conditions are recorded every 30 minutes by the CANDHIS network at the Leucate buoy moored 2.1 nautical miles off the study area (in front of the weather station, **Fig. 1**) at a depth of 40 m (Cerema et al., 2019).

The wave energy density E (in J/m²) is calculated, according to the linear wave theory (1) :

$$E = \frac{1}{8}\rho g H_{m0}^2 \quad (1)$$

Where H_{m0} is the spectral significant wave height.

The hourly averaged wind data come from the Météo France weather station of Cape Leucate semaphore (**Fig. 1**) located about 2.5 km from the study sites at a height of 42 m above sea level.

Hourly water level (WL) measurements are taken from the tide gauge located in Port-Vendres (45 km south of the study site). To evaluate the extent of the marine influence on the beach, the 2 % exceedance value of run-up on the beach face ($R_{2\%}$) is computed using Stockdon et al.'s (2006) empirical formula (2):

$$R_{2\%} = WL + \left[1.1 + \left(0.35\beta_f (H_0 L_0)^{1/2} + \frac{\left[H_0 L_0 \left(0.563\beta_f^2 + 0.004\right)\right]^{1/2}}{2}\right)\right] \quad (2)$$

where WL is the water level, H_0 is the deep water wave-height, L_0 the deep-water wave length and β_f the beach slope from Aleman et al., 2015.

4. Results

4.1 Forcing conditions

Weather pattern statistics during the survey period (2017-2020, **Fig. 5**), are consistent with long-term statistics (2007-2020, **Fig. 1**). Globally, the summer period is the least energetic, with an Hs value around 1 m (≈ 50% of the time) and mean wind velocity lower than 10 $m.^{-1}$ most of the time (**Fig. 5**). The winter period is more energetic, with possible waves higher than 2 m (2% of the time) and mean wind velocity over 10 $m.s^{-1}$ and up to 27 $m.s^{-1}$ (**Fig. 5**).

Two main types of weather pattern can be distinguished: 1) dominant offshore conditions with an NW wind (73% of the time) and 2) less common onshore wind conditions (27% of the time) but rather energetic because accompanied by waves that can exceed 2.5m. These two main forcing conditions can be subdivided as following (**Tab. 1 and Fig. 6**):

Most of the time (41%), strong offshore winds generate offshore-directed waves (**Tab. 1 and Fig. 6b**), that does not impact the study sites and escape the Gulf of Lions. In some cases (29% of the time), the offshore wind can be paired with onshore waves of less than 1 m. Offshore conditions occur throughout the year, but are more energetic in winter (**Fig. 5**), when the mean wind can reach speeds of around 15 $m.s^{-1}$ for several days, i.e. from 04/01/2019 to 12/01/2019, the average daily offshore wind speed was 12 $m.s^{-1}$ (gusts reaching over 30 $m.s^{-1}$). Offshore wind conditions accompanied by onshore waves higher than 1 m are not discussed further here, as these forcing conditions are developed in a minority of cases and correspond to only short transitional states.

The most common onshore forcing conditions are low-amplitude waves (Hs<1 m) accompanied by sea breezes (25% of the time), while storm conditions with Hs greater than 2 m, usually accompanied by onshore winds, are the least common (2% of the time) (**Tab. 1 and Fig. 6c**). Storms are common during the winter period (**Fig. 5**), and can reach Hs > 6 m, Hmax> 8 m (for a wave energy flux over $30*10^3$ J/m) with wind speeds > 20 $m.s^{-1}$ on daily average (i.e. 06/03/2018). Water-level measurements show large variations in winter linked to storm surges (that can reach 0.2 m to 0.6 m).

Finally, 97% of the forcing conditions can be summarised according to 5 forcing situations: (1) offshore wind alone were sea-breezes and waves are cancelled, 41% (Light blue, **Tab. 1**); (2) offshore wind and small waves < 1m, 29% (Dark blue, **Tab. 1**); (3) onshore fair-weather waves < 1 m, 20% (Green, **Tab. 1**); (4) onshore waves between 1 and 2 m, 5% (Orange, **Tab. 1**) and (5) onshore storm waves > 2 m, 2% (Red, **Tab. 1**).

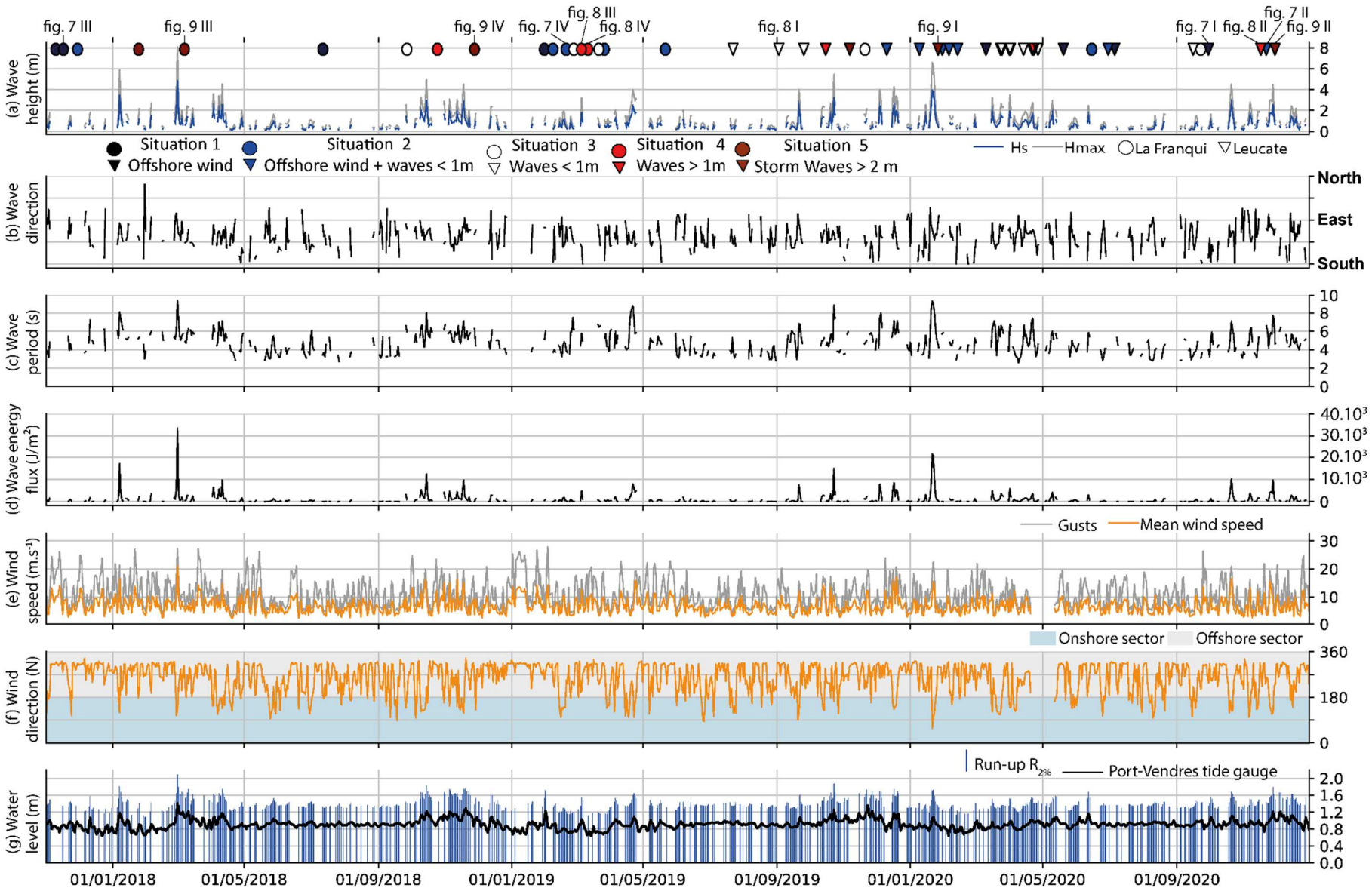
fig. 7 III
fig. 9 III
fig. 9 IV
fig. 7 IV
fig. 8 III
fig. 8 IV
fig. 8 I
fig. 9 I
fig. 7 I
fig. 8 II
fig. 7 II
fig. 9 II
(a) Wave height (m)
Situation 1
Offshore wind
Situation 2
Offshore wind + waves < 1m
Situation 3
Waves < 1m
Situation 4
Waves > 1m
Situation 5
Storm Waves > 2 m
Hs
Hmax
La Franqui
Leucate
(b) Wave direction
North
East
South
(c) Wave period (s)
(d) Wave energy flux (J/m²)
Gusts
Mean wind speed
(e) Wind speed (m.s⁻¹)
Onshore sector
Offshore sector
(f) Wind direction (N)
Run-up R2%
Port-Vendres tide gauge
(g) Water level (m)
01/01/2018
01/05/2018
01/09/2018
01/01/2019
01/05/2019
01/09/2019
01/01/2020
01/05/2020
01/09/2020

251

252

253 *Figure 5. Time series of recorded daily: a) wave heights; b) wave direction; c) wave period; d)*
254 *wave energy density (periods of offshore waves are not indicated for sake of clarity); e) hourly mean*
255 *wind speed and gusts; f) hourly mean wind direction; g) water levels. The red line is the Port-Vendres*
256 *tide gauge and the blue bars are the calculated run-up height (all levels are in metre NGF, French*
257 *official topographic reference). The surveys are shown at the top of the first graph (a) with circles for*
258 *La Franqui beach and triangles for Leucate beach. The colour scale indicates the dominant forcing*
259 *condition prior to the survey: black refers to surveys influenced by offshore winds, blue to offshore*
260 *wind conditions concomitant with waves < 1 m, white to waves < 1m with onshore wind or no wind,*
261 *red to waves > 1m and brown to storm events (onshore influence).*
262

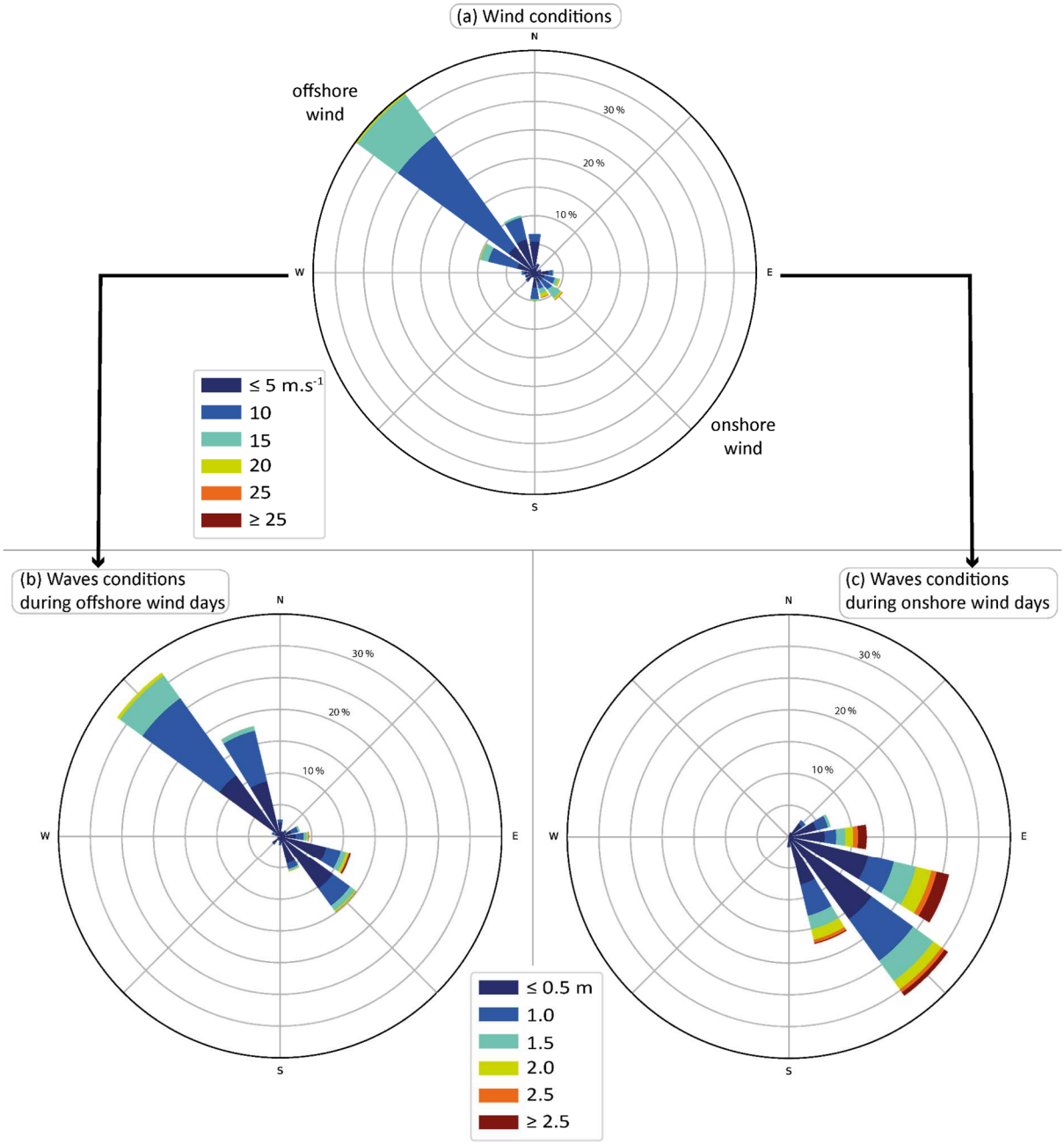

263
264

265

266 *Figure 6. (a) Wind conditions during the study period 2018-2020; (b) wave directions and*
267 *heights during offshore wind events; (c) wave conditions during onshore wind events.*
268

269 *Tab 1. Forcing conditions and their occurrence (percentage of time), computed from the*
270 *Leucate buoy and weather station data*

Wind		Waves			
Dir.		Dir.	Hs<1m	1m<Hs<2m	2m>Hs
Offshore	73%	Offshore	41%		
		Onshore	29%	3%	
Onshore	27%	Onshore	20%	5%	2%

4.2 Morphological evolution

The established scale of forcing conditions (**Tab. 1**) is used to describe the observed backshore morphology response as a function of the 5 forcing conditions: (situation 1) offshore wind alone were sea-breezes and waves are cancelled; (situation 2) offshore wind and small waves < 1m; (situation 3) onshore waves < 1 m (fair weather); (situation 4) onshore waves between 1 and 2 m; and (situation 5) onshore waves > 2 m (storm conditions). In each subsection below, one example for Leucate beach and one for La Franqui beach are presented for each situation, in the form of two differential maps per site, accompanied by two topographic sections showing the evolution of the beach at a horn and an embayment (**Fig. 7, 8, 9**). These examples are representative of the main morphological changes observed under similar forcing conditions for each case (**Tab. 2, 3, 4**). Finally, tables summarise all the observations made on each of the two sites for each situation (**Tab. 2, 3, 4**), based on the 44 DEM measured. This allows us to reach a conclusion on the main morphological evolutions observed for each situation.

4.2.1 Offshore wind conditions (situation 1 & 2)

For situation 1 the offshore wind is the only forcing agent, sea-breezes and waves are not present, as in Leucate from 17/09/2020 to 01/10/2020 (see differential map **Fig. 7 I**), with an average hourly speed of 6.3 $m.s^{-1}$ (maximum hourly average 17.2 $m.s^{-1}$, maximum gust 34 $m.s^{-1}$) (**Fig. 5**). At La Franqui (**Fig. 7 III**), from 09/11 to 16/11/2017 the average hourly speed was 9.6 $m.s^{-1}$ (maximum hourly average of 17.5 $m.s^{-1}$, maximum gust 32 $m.s^{-1}$) (**Fig. 5**). The sediment is transported towards the beach face creating an accretion (respectively for each site +0.2 / +0.4 m), and leading to a strong uniform advance of the coastline by up to +10 m for the two beaches (see profiles **Fig. 7 a, c, e, g**). While the backshore is eroded up to -0.3m and losing around -0.2m^3/m^2 (**Fig. 7 I, III**), a zone of slight accretion is observed at the foredune foot on Leucate beach, up to +0.1 m^3/m^2 (**Fig. 7 I**) and very locally in some depression zones of the beach of La Franqui (+0.2 m^3/m^2). The same observations are made

298 for all the periods in situation 1 (41% of the time **Tab.1**), namely 5 times at Leucate and 4
299 times at La Franqui (**Tab. 2**).
300 In the situation 2 the main forcing is the offshore wind paired with a small onshore waves
301 (Hs <1 m), as in Leucate, from 18 to 23/11/2020 (**Fig. 7 II**), with an average hourly speed of
302 5.3 $m.s^{-1}$ (maximum: 14.2 $m.s^{-1}$, maximum gust 27 $m.s^{-1}$) paired with a small onshore waves
303 Hs <1 m (total wave energy flux over the entire period: $3.9*10^3$ J/m; with a peak flux of
304 $0.7*10^3$ J/m per hour) (**Fig. 5**) where maximum run-up height is $R_{2\%}$ = 0.68 m, which
305 corresponds to the berm crest level. At La Franqui, from 07/02 to 20/02/2019 (**Fig. 7 IV**),
306 offshore wind is an average hourly speed of 5.3 $m.s^{-1}$ (maximum: 12 $m.s^{-1}$, maximum gust 25
307 $m.s^{-1}$) combined with a small onshore waves Hs <1 m (total wave energy flux over the entire
308 period: $13.5*10^3$ J/m; with a peak flux of $4*10^3$ J/m per hour) (**Fig. 5**) with maximum run-up
309 height $R_{2\%}$ = 0.73 m, which corresponds to the berm crest. The backshore is also eroded for
310 the two beaches, up to -0.3m corresponding to -0.3 m^3/m^2 on the whole backshore (**Fig. 7 II,**
311 **IV**). The beach face morphologies show a clear longshore pattern, horns positions shows a
312 seaward advance of the shoreline of a few metres, associated with beach-face accretion that
313 can reach + 0.4 m^3/m^2 (**Fig. 7 d, h**). On the other hand, the position of the embayments shows
314 a landward retreat of a few metres and the beach face is in erosion, losing around -0.2m^3/m^2
315 (**Fig. 7 b, f**). Similar observations are made, for all the periods of situation 2 (29% of the time
316 **Tab.1**), namely 6 times at Leucate and 8 times at La Franqui (**Tab. 2**).

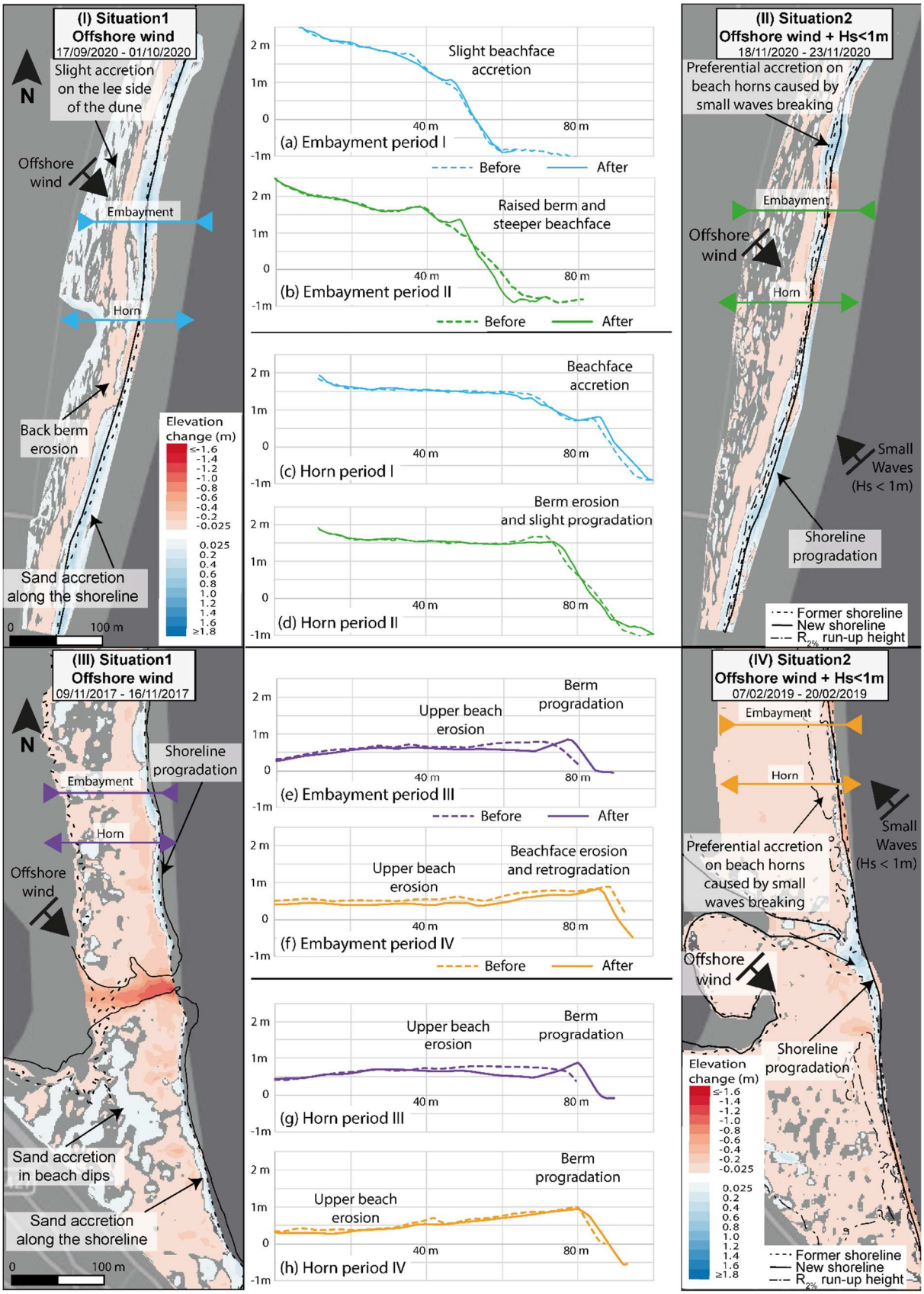

Figure.7. Morphological evolutions on Leucate beach (top) and La Franqui (bottom), for offshore wind periods (I, a, c & III, e, g) and for periods combining offshore wind and onshore waves Hs<1 m

(II, b, d & IV, f, h). Dotted profiles correspond to the initial profile and solid profiles to the final situation.

Tab.2. Summary of all the morphological evolutions observed following episodes of offshore wind (11 observations/44) and offshore wind combined with waves Hs<1 m (13 observations/44) at Leucate and La Franqui beaches. Shl. Stands for shoreline.

Forcing condition	Site	Date	Backshore	Embayment	Horn
Situation 1 Offshore wind	Leucate	11/03/20, 21/05/20, 07/07/20, 01/10/20	Back berm eroded, up to -0.2 m. Dune foot accretion up to +0.1 m	-Shl. advance up to +5 m -beach face accretion up to +0.3m -stable berm	-Shl. advance up to +8 m -beach face accretion up to +0.4m -slight berm accretion
	La Franqui	09/11/17, 16/11/17, 12/07/18, 31/01/19, 27/01/22, 31/01/22, 03/02/22	Eroded up to -0.3 m	-Shl. advance up to +8 m -beach face accretion up to +0.4m -well marked berm	-Shl. advance up to +10 m -beach face accretion up to +0.3m -well marked berm
Situation 2 Offshore wind + Hs<1m	Leucate	11/12/19, 10/01/20, 31/01/20, 06/02/20, 14/02/20, 01/07/20, 23/11/20	Back berm eroded, up to -0.2 m. Dune foot accretion up to +0.1 m	-Shl. retreat up to -2 m -steeper beach face, collision slope erosion up to -0.3 m -raised berm +0.3 m	-Shl. advance of the shoreline up to +2 m -beach face accretion/advance up to +0.3 m -eroded top berm top -0.2m
	La Franqui	29/11/17, 08/02/19, 20/02/19, 27/03/19, 22/05/19, 16/06/20	Eroded up to -0.3 m	-Shl. retreat up to -5 m -beach face erosion up to -0.4m -stable berm	-Shl. advance up to +6 m -stable beach face slope -slight berm accretion

4.2.2 Onshore wind conditions

The following results are presented in two main parts, drawing a distinction between fair-weather conditions (Hs< 1 m, situation 3 and Hs =1-2 m, situation 4) and high-energy storm conditions (Hs> 2m, situation 5).

Hs< 1 m (situation 3) and Hs =1-2 m (situation 4)

The situation 3 is characterised by significant waves height under 1 m of frontal incidence (fair weather waves). For example, at Leucate from 23/07/2019 to 03/09/2019 (**Fig. 8 I**), where the period is characterised by average Hs around 0.4 m (total wave energy flux over the entire period: $70*10^3$ J/m; with a peak flux of $3*10^3$ J/m per hour) (**Fig. 5**). The run-up height was $R_{2\%}$= 0.76 m, which corresponds to the berm crest. During this period, the average hourly wind speed is around 5.5 $m.s^{-1}$ coming from the W/NW sector (maximum gust 15 $m.s^{-1}$) (**Fig. 5**). At La Franqui, from 20/02/2019 to 27/02/2019 (**Fig. 8 III**), with average Hs around 0.5 m (total wave energy flux over the entire period: $4.2*10^3$ J/m; with a peak flux of $0.5*10^2$ J/m per hour) (**Fig. 5**). The run-up height was $R_{2\%}$= 0.73 m, which corresponds to the berm crest. During this period, the average hourly wind speed is around 3 $m.s^{-1}$ coming from the SW sector (maximum gust 13 $m.s^{-1}$) (**Fig. 5**). The morphological responses for horns and embayments on both locations are similar to the situation 2 (**Fig. 8 I, III**). The embayments show signs of erosion, with a retreat of up to -5 m and erosion of the beach face and berm (-0.3m^3/m^2) (**Fig. 8 a, e**). By contrast, the horns are accreting, associated with an advance of the shoreline of up to +5 m, while the beach face shows an accretion of + 0.3 m (+ 0.3m^3/m^2) and the berm remains relatively stable (**Fig. 8 d, g**). Similar morphological changes are observed for all periods in situation 3 (20% of the time **Tab.1**), namely 4 times at Leucate and 4 times at La Franqui (**Tab. 3**).

The situation 4 is characterised by Hs over 1 m. For example, at Leucate, from 01/10/2020 to 18/11/2020 (**Fig. 8 II**), where the period is characterised by two events with Hs remained around 2 m (total wave energy flux over the entire period: $47.2*10^4$ J/m; with a peak flux of $9*10^3$ J/m per hour). The first event lasted for more than 12 h, while the second one was shorter (**Fig. 5**). The run-up height $R_{2\%}$ for these two events is 0.90 m, which allows only overtopping of the berm. During these two events, the maximum hourly wind speed is around 16 $m.s^{-1}$ coming from the S/SE sector (maximum gust 22 $m.s^{-1}$) (**Fig. 5**). At La Franqui, from 27/02/2019 to 13/03/2019 (**Fig. 8 IV**), with Hs of around 2 m for more than 10 h (total wave energy flux over the entire period: $14*10^4$ J/m; with a peak flux of $5.7*10^3$ J/m per hour) (**Fig. 5**) and run-up height $R_{2\%}$ = 0.84 m, which allows also overtopping of the berm. During this period, the maximum hourly wind speed is around 11 $m.s^{-1}$ coming from the S sector (maximum gust 15 $m.s^{-1}$) (**Fig. 5**). The shorelines record respectively a retreat of between -5 and -15 m (**Fig. 8 II, IV**), and the berms become raised and well-marked (up to + 0.6 m^3/m^2 of accretion) (**Fig. 8 b, d, f, h**). This can lead to a steeper beach face (**Fig. 8 b, d**). The

backshore is slightly affected by these changes due to the low surge level. The same observations are made for all the periods in situation 4 (5% of the time **Tab.1**), namely both 3 times at Leucate and at La Franqui (**Tab. 3**).

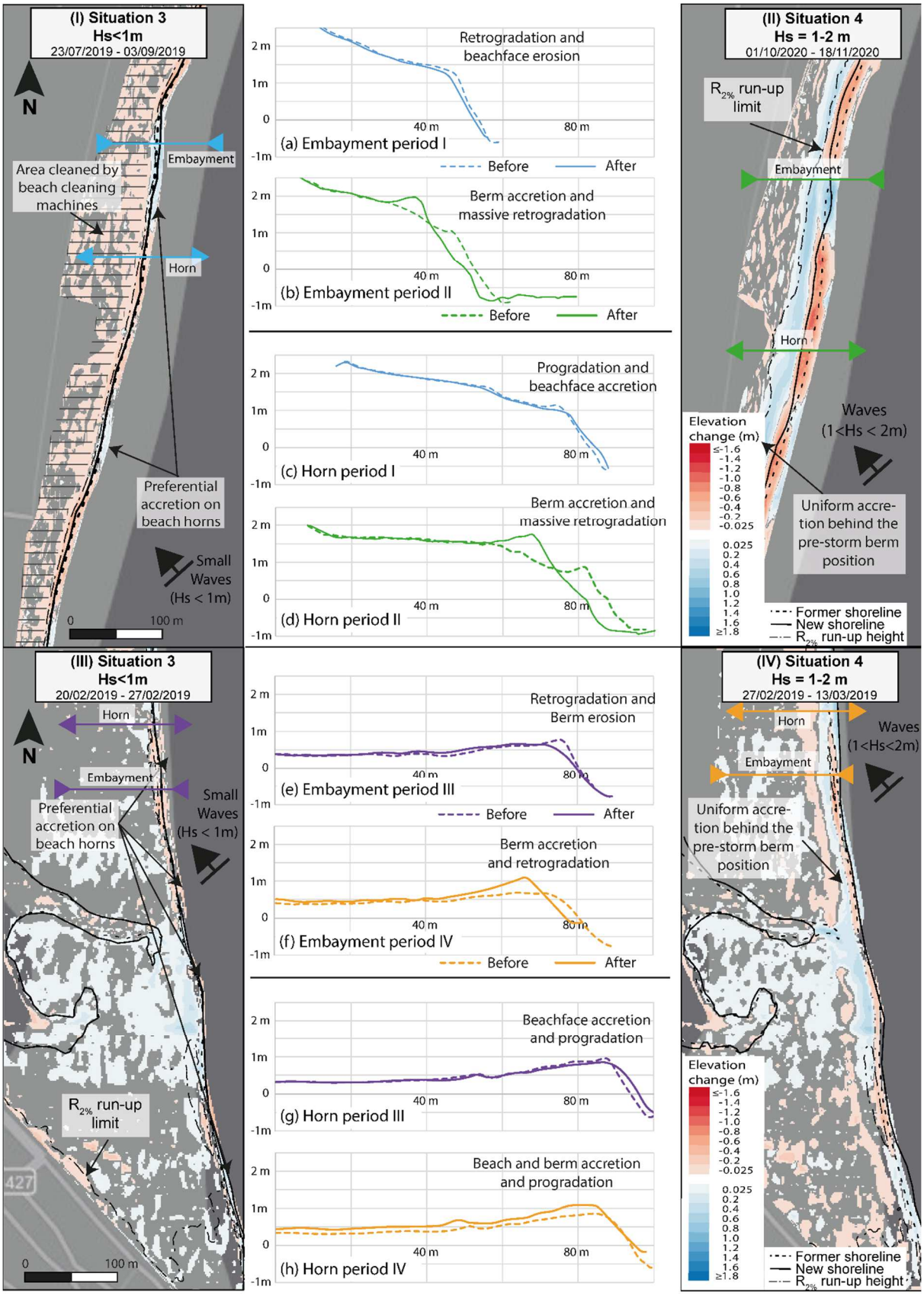

Figure.8. Morphological evolutions on the beaches of Leucate (top) and La Franqui (bottom), for onshore-wave periods with Hs<1 m (I, a, c & III, e, g) and for onshore-wave periods with Hs = 1-2 *m (II, b, d & IV, f, h). Note that (I) the backshore is actively cleaned by the passage of a Beach Cleaning machines towed by tractors, and is not affected by the morphological evolution of the shoreline. Dotted profiles correspond to the initial profile and solid profiles to the final situation.*

Tab.3. Summary of all the morphological evolutions observed following wave episodes with Hs<1 m (8 observations/44) and with Hs = 1-2 m (6 observations/44) observed on Leucate and La Franqui beaches. Shl. Stands for shoreline.

Forcing condition	Site	Date	Backshore	Embayment	Horn
Situation 3 Hs <1 m	Leucate	23/07/19, 03/09/19, 26/09/19, 17/09/20	Stable	-Shl. retreat up to -3 m -beach face erosion up to -0.3m -berm less marked	-Shl. advance up to +5 m -beach face accretion up to +0.3m -stable berm
	La Franqui	27/02/19, 27/09/18, 22/03/19, 21/11/19	Slight accretion	-Shl. retreat up to -5 m -beach face less steep -berm erosion up to -0.3 m	-Shl. advance up to + 4 m -beach face accretion up to +0.3m -stable berm
Situation 4 Hs = 1-2 m	Leucate	16/10/19, 24/04/20, 18/11/20	Stable dune foot	-Shl. retreat up to -10 m -steeper and raised beach face up to +0.3 m -massive retreat of the shoreline	-Shl. retreat up to -15 m -steeper and raised beach face up to +0.9 m -massive retreat of the shoreline
	La Franqui	12/03/19, 25/10/18, 06/03/19	Stable	-Shl. retreat up to -5 m -stable beach face slope-berm retreat up to -6 m, raised up to +0.6 m	-Shl. retreat up to -5 m -stable beach face -berm retreat up to -6 m, raised up to +0.6 m and beach accretion along the profile

Storm conditions (Hs> 2m) (situation 5)

In Leucate for situation 5 where the main forcing agent is an easterly storm, such as between 10/01/2020 and 27/01/2020 (**Fig. 9 I**), with Hs> 4 m during 30 h (total wave energy flux over the entire period: $12.96*10^5$ J/m; with a peak flux of $34*10^3$ J/m per hour) and a maximum around 8 m (the main peak on 23/01/2020, **Fig. 5**) and corresponding run-up height is $R_{2\%}$ = 1.80 m, which corresponds to the foot of the dune, the beach is submerged. During this storm event, the maximum hourly wind speed is around 15 $m.s^{-1}$ coming from the S/SE sector (maximum gust 22 $m.s^{-1}$) (**Fig. 5**). Another example occurs in Leucate from

388 23/11/2020 to 01/12/2020 (**Fig. 9 II**) when an easterly storm, with an Hs> 2 m during 3 days
389 and a maximum of around 6 m (total wave energy flux over the entire period: $30.8*10^4$ J/m;
390 with a peak flux of $10*10^3$ J/m per hour) (**Fig. 5**) with the Run-Up height of $R_{2\%}$ = 1.47 m,
391 which corresponds to the back of the pre-storm berm. During this storm event the maximum
392 hourly wind speed is around 15 $m.s^{-1}$ coming from the SE sector (maximum gust 19 $m.s^{-1}$)
393 (**Fig. 5**). Following these two major storm events at Leucate, large quantities of sediment are
394 deposited on the backshore (+ 0.5 m^3/m^2) around the maximum submergence limit which
395 reaches the foot of the dune (**Fig. 9 I, II**). This boundary shows a longshore variability in
396 relation to the position of the horns (**Fig. 9 I, II**) which are topographically lower and less
397 sloping than the embayments (**Fig. 9 a,c & b,d**). Sediment deposition is therefore slightly
398 more important on the backshore behind the horns. A new berm is formed in a landward
399 position with a higher altitude along the horns, whereas the berm is just over-raised along the
400 embayments (+ 0.3m). This result in a straighter and higher berm. The position of the
401 shoreline is relatively constant given the forcing conditions. The same observations are made
402 for all periods in situation 5 (5% of the time **Tab.1**), that is, a total of 3 times in Leucate
403 (**Tab. 4**).
404 At La Franqui for situation 5, a major easterly storm of decadal recurrence, occurs
405 between the 24/01/2018 and 07/03/2018 (Fig. 8 III), (storm peak : 01/03/2018 to 02/03/2018,
406 reaching $34*10^3$ J/m in a day **Fig. 5**), with an Hs> 6 m during 40 h and maxima of around 10
407 m (total wave energy flux over the entire period: $82.4*10^4$ J/m; with a peak flux of 34.10^3 J/m
408 per hour); the run-up height is $R_{2\%}$=2.4 m (**Fig. 5**), the beach is fully submerged. During this
409 storm event the maximum hourly wind speed is around 20 $m.s^{-1}$ coming from the SE sector
410 (maximum gust 27 $m.s^{-1}$) (**Fig. 5**). From 27/09/2018 to 28/11/2018 (**Fig. 9 IV**), La Franqui
411 beach experiments also an easterly storm of lesser intensity (peak on 17/11/2018, $10*10^3$
412 J/m), with Hs>2 m during 36 h and maxima of around 6 m (total wave energy flux over the
413 entire period: $91*10^3$ J/m; with a peak flux of $10*10^3$ J/m per hour) with the maximum run-
414 up height of $R_{2\%}$= 1.4 m, which indicates that the beach becomes completely submerged.
415 During these storm events the maximum hourly wind speed is around 15 $m.s^{-1}$ coming from
416 the SE sector (maximum gust 20 $m.s^{-1}$) (**Fig. 5**). Deposition occurs over the entire backshore
417 (up to +0.8 m, corresponding to + 0.8 m^3/m^2) (**Fig. 9 III, IV**) and extends into the lagoon.
418 The formation of the new well-marked berm in retreat on the beach concentrates most of the
419 sediment input (up to +0.7m, corresponding to + 0.8 m^3/m^2) (**Fig. 9 III, IV**). In some cases,
420 washover cones are formed (**Fig. 9 III**). The coastline, on the other hand, shows major retreat

of the shoreline and linearization. Similar observations are made for all periods in situation 5 (5% of the time **Tab.1**), that is, a total of 3 times in La Franqui (**Tab. 4**).

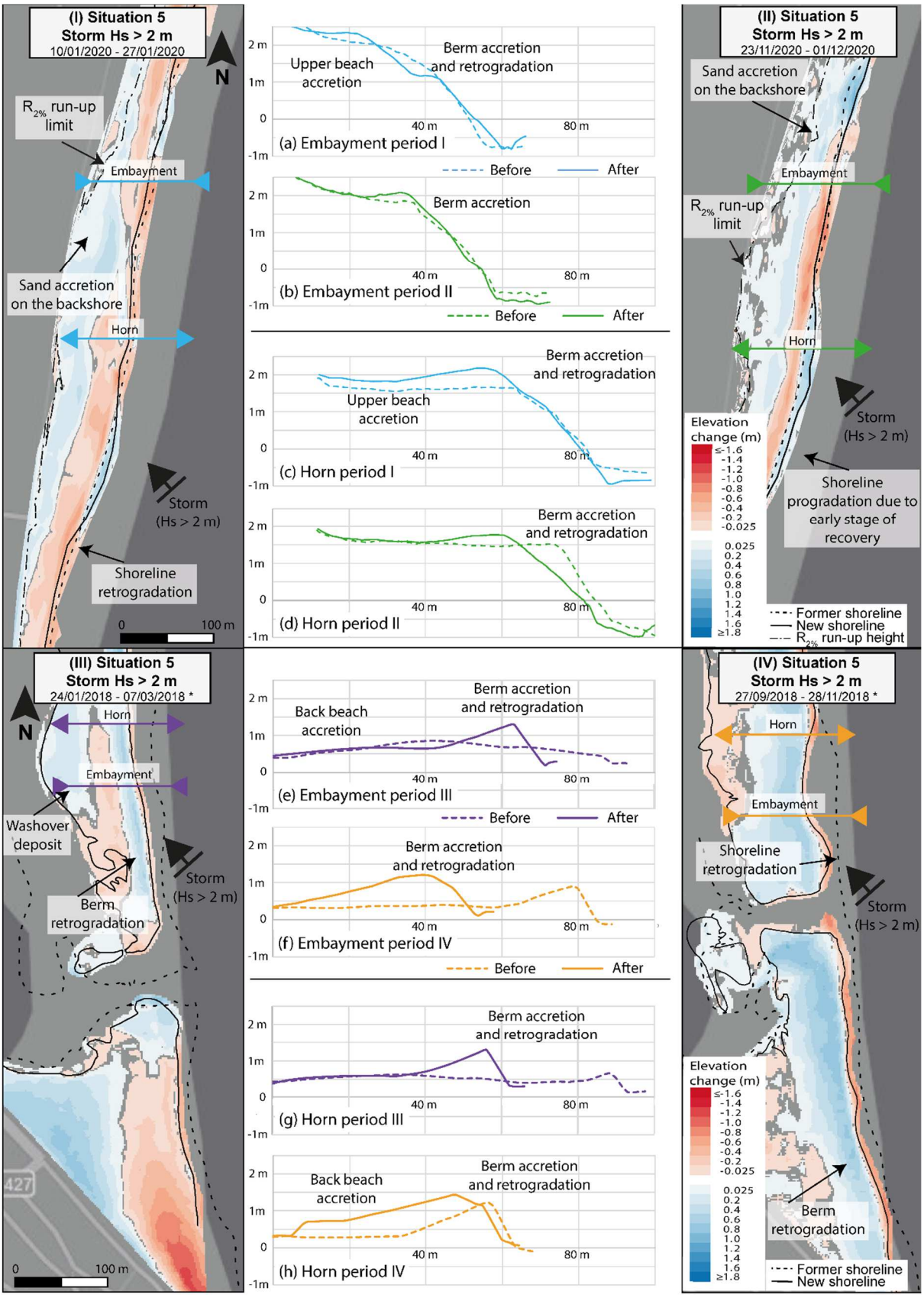

*Figure.9 Morphological evolutions on the beaches of Leucate (top) and La Franqui (bottom). For storm periods of annual recurrence (I, a, c; II, b, d & IV, f, h) and for a storm of decadal recurrence at the La Franqui (III, e, g). Dotted profiles correspond to the initial profile and solid profiles to the final situation. *The beach is completely submerged during storms.*

Tab. 4. Summary of all the morphological evolutions observed following storm events (6 observations/44) observed on Leucate and La Franqui beaches (Fig. 7). Shl. Stands for shoreline.

Forcing condition	Site	Date	Backshore	Embayment	Horn
Situation 5 Hs> 2 m (Storms)	Leucate	07/11/19, 27/01/20, 01/12/20	Sedimentation on the backshore around max. submergence limit up to +0.5 m	-globally stable Shl. respecting high forcing -steeper beach face -berm raised up to +0.4 m	-Shl. retreat -beach face less steep or stable -berm retreat up to -15 m, raised up to +0.5 m
	La Franqui	24/01/18, 28/11/18, 07/03/18	Completely submerged with accretion and washover deposits	-Shl. retreat, up to -20 m -steeper beach face -berm raised up to +0.7 m	-Shl. retreat, up to -25 m -steeper beach face -berm raised up to +0.7 m

5. Discussion

5.1. Morphodynamics evolutions of two Mediterranean beaches presenting permanent megacusps

Several conceptual models of beach evolution can provide a rough classification of beach states (e.g. Castelle et al., 2007; Lippmann and Holman, 1990; Masselink and Short, 1993; Short and Woodroffe, 2009; Wright and Short, 1984), but they mostly focus on the dynamics of the nearshore area and little on the emerged beach. They do not provide a detailed understanding of the morphological changes generated by forcing conditions. Here, a conceptual morphodynamic model is proposed for the two studied Mediterranean low-microtidal beaches presenting permanent megacusps. It summarises the different forcing parameters and their morphological impacts on the emerged beach, based on the observations of 44 DEM during four years of survey:

- The first situation is dominated only by offshore wind, sea breezes, tides and waves are cancelled (**Fig. 10 a**). The result is a significant aeolian transport inducing an erosion on the upper beach down to -0.3 m (see **Fig. 7 f,h**), as well as an accretion on the shoreline (about + 0.4 m for the beach face) leading to a uniform seaward migration of the shoreline (**Fig. 10 I a, b**). This first situation purely driven by offshore wind occurs preferentially in autumn and winter, when such winds are frequent (**Fig. 11**) with high intensity. Although this situation is common, several obstacles can modulate the imprint of this process: 1) The presence of a dune that can slow down or disturb the flow (Bauer et al., 2012; Delgado-Fernandez et al., 2013; Jackson et al., 2013; Lynch et al., 2013; Walker and Shugar, 2013). This latter effect is particularly visible when comparing the 2 sites, at Leucate a light erosion zone is visible at the dune foot (**Fig. 10 II a, b**) whereas at La Franqui in the absence of a dune the erosion on the upper beach is general (**Fig. 10 I a, b**); 2) Foredunes are also often stabilised by vegetation or a fence preventing the free exchange of sediments with the rest of the beach (Itzkin et al., 2020; Nordstrom, 2021; Robin et al., 2020; Walker et al., 2022); 3) In addition, surface moisture due to the proximity of the water table or climatic condition can also slow down or prevent the aeolian sediment transport by aggregating the grains of sand together (Davidson-Arnott et al., 2008; He et al., 2022; Jackson and Nordstrom, 1997; Li et al., 1997; Namikas et al., 2010). This latter effect should be taken in consideration, especially on low-lying beaches such as La Franqui (**Fig. 10 I a, b**) where the presence of moisture at a depth of a few centimetre (derived from the capillary fringe of the water table) acts as a constraint limiting beach erosion.

- The second situation (**Fig. 10 b**) is quite common throughout the year (**Fig. 11**), it arises from the coupled action of offshore winds and very low amplitude waves (Hs< 1 m). There is sediment accretion on the horns while the embayments are only slightly eroded. In this situation, the seaward migration of the horns can reach its maximum (up to 6 m). Field observations suggest that this dynamic is due to the refraction of waves according to the shape of the coastline, the seaward extension of the horns leading to the convergence of the waves and their breaking on the horns (e.g. Falqués et al., 2021), thus attenuating their energy, while it is maximal in the bays. The morphodynamic of the emerged beach is similar to that described for the first situation (**Fig. 10 a**).

- The third situation (**Fig. 10 c**) corresponds to low-intensity waves (Hs<1 m) without wind. This situation is frequent, particularly in summer (**Fig. 11**). Morphological changes on the beach face are similar to those described in situation 2 (**Fig. 10 b**), with accretion

478 inducing advance of the horns, due to refraction of small waves on the salient and slight
479 erosion inducing potential retreat of the embayments.
480 - The fourth situation (**Fig. 10 d**) shows the effect of moderate-intensity waves (Hs> 1 m)
481 that mostly occurs in autumn and spring (**Fig. 11**). When the run-up limit overtops the berm,
482 it results in a homogeneous landward migration of the beach face, the narrowing of the beach
483 and the formation of a higher berm with a steeper beach face.
484 - The fifth situation (**Fig. 10 e**) is associated with morphological changes induced by storm
485 conditions (Hs> 2 m) inducing a partial or total submersion of the emerged beach. The beach
486 face is eroded, the coastline migrates landward and a new higher berm with a steeper beach
487 face is established in a retreated position. In the case of the low-lying beach of La Franqui
488 where the backshore is not backed by a dune (**Fig. 10 Ie**), the beach is easily submerged due
489 to its low elevation and sediments are deposited on the backshore or on the lagoon in the
490 form of washover fans. In cases where the beach is backed by a dune like Leucate (**Fig. 10**
491 **IIe**), sediments can be deposited at the foot of the dune, and erosion notches are observed
492 only locally. Similar dynamics are commonly observed on other sites (Eichentopf et al.,
493 2019b; Karunarathna et al., 2014; Sallenger, 2000). This fifth situation predominantly occurs
494 during the winter months (**Fig. 11**).
495 At a yearly scale, the balance between periods of erosion and accretion is generally
496 attributed to seasonal variability, with winter being rather energetic and erosive (Casamayor
497 et al., 2022; Dolique et al., 2019; Quartel et al., 2008; Wright and Short, 1984). During the
498 summer period, there is an alternation between situations 1, 2, 3 (Fig. 11 a, b, c). Winter is
499 marked by periods of strong offshore winds (situation 1; Fig. 11 a, b) punctuated by brief
500 energetic events (situations 4; Fig. 11 d) or storms (situation 5; Fig. 11 e). The constructive
501 small waves (situation 2 and 3; Fig. 11 b, c) can participate in a partial reconstruction of the
502 beach face (Bugajny and Furmańczyk, 2020). The sediment supply on the emerged beach by
503 storm episodes can be remobilized by offshore wind events (situation 1 and 2; Fig. 11 a, b)
504 and contribute to induce a new seaward migration of the shoreline.

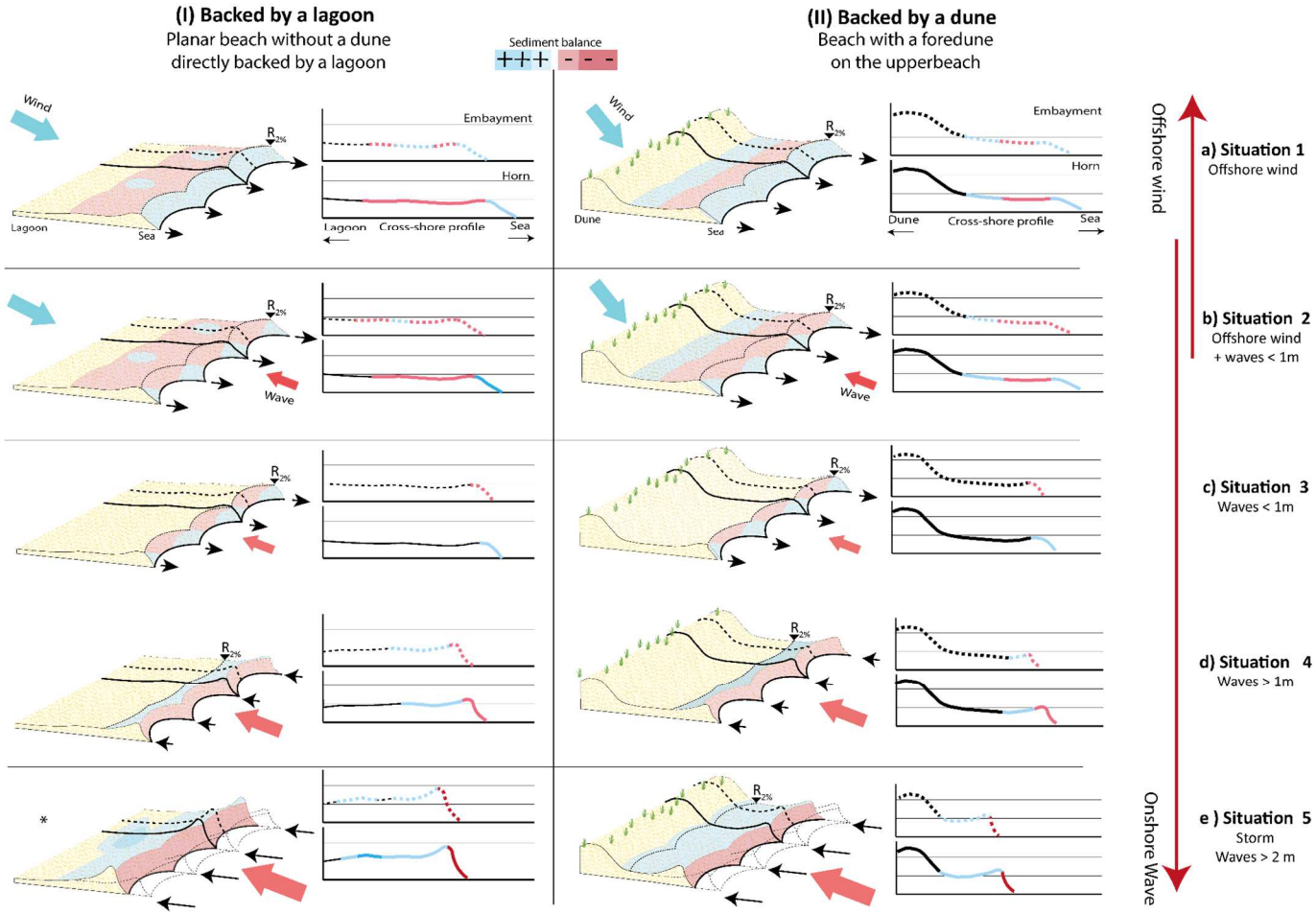

Figure.10 Morphological model of beach evolution for a beach backed by a lagoon with a planar upperbeach profile, La franqui (I) and with a dune, Leucate (II). $R_{2\%}$ marks the maximum limit of the Run-Up. Dotted profiles correspond to embayments and solid profiles to the horns. (*) the beach is totally submerged by the storm.

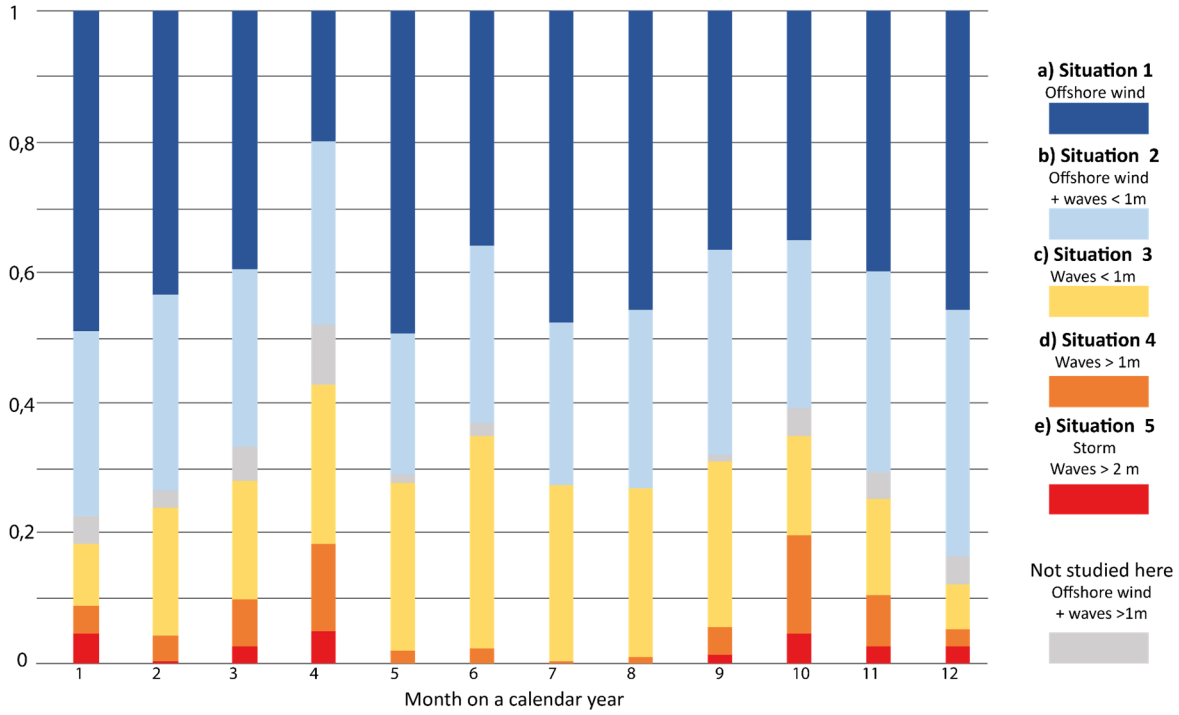

Figure.11 Monthly occurrences for each of the five forcing conditions, over the period ranging from 2006 to 2021

5.2 Morphodynamic specificities of the two Mediterranean beaches

The conceptual model proposed in **Fig.10** for both study sites fits globally with the observations made for other microtidal environments worldwide. However, some significant particularities can be highlighted: 1) the low-microtidal context has a significant impact on the morphodynamic of the beach face during fair-weather or storm conditions, and 2) The role of the offshore wind is major.

1- At the study sites, the sea level is relatively constant over time and thus the intertidal zone is very narrow. The maximal tidal range of 0.3 m induces an intertidal zone width of around 3 m at Leucate. However, a tidal range of 2 m on an identical beach face slope would produce an intertidal zone at least 26 m wide. The relative static position of the sea level has important consequences on the morphodynamics of the beaches. Firstly, the morphological changes induced by fair-weather conditions are clearly visible and concentrated on the beach face. The coastline can migrate several metres in a few days, either uniformly under the effect of offshore wind sediments inputs (situation 1 **Fig.10**), or only on the horns under the action of fair-weather waves while embayments may show minor erosion or stability (situation 2, 3 **Fig.10**). Fair-weather conditions are common and persist for long periods, nearly 90% of the

time (**Tab. 1**), this explains dominance of these situations in the conceptual beach model (situation 1, 2, 3 **Fig.11**). The sea level remaining practically static allows even the weakest hydrodynamic processes to take place on the beach faces without being disturbed by the tidal sweep as in higher tidal range environment (Bertoni et al., 2013; Cooper, 1994; Sedrati et al., 2009; Short and Aagaard, 2020). Secondly, during moderate-intensity waves episodes (situation 4, **Fig.10 d**), the low tidal range may also allow the high run-up level to stabilise for a longer period of time in a high elevation on the backshore. This can lead to the retreat and elevation of the berm, creating generally a massive berm. During more energetic storm episodes (situation 5, **Fig.10 e**), a new wider berm with higher height and relatively uniform crest elevation along the crescentic coastline may be established in a remote position on the backshore (Armaroli et al., 2013; Durán et al., 2016; Gervais, 2012; Gervais et al., 2010). At microtidal sites with a larger tidal range (≈ 2m), berm seems to be of smaller size even after storms episodes (see for comparisons: Karunarathna et al., 2014; Ruiz de Alegría-Arzaburu et al., 2022). At our sites, there is also some sediment accretion on the upper beach during storm-induced flooding events, either along the toe of the dune (situation 5, **Fig.10 IIe**) or behind the dune in extreme cases. At microtidal sites with a larger tidal sweep, these storm deposits along the dune foot are thinner compared to what is observed at the study sites (see for comparisons: Eichentopf et al., 2019b; Karunarathna et al., 2014; Leatherman, 1979). In the case of a low-lying beach (e.g. La Franqui), the overwash regime is reached even for low-intensity storms (Sallenger, 2000). This can result in washover deposits (situation 5, **Fig.10 Ie**) that are accumulated in poorly vegetated areas or in lagoons (Balouin et al., 2005; Durán et al., 2016; Sabatier et al., 2008; Sedrati et al., 2011). This process can potentially provide a stockpile of sand available to feed the beach face and the nearshore during future offshore wind events.

2**-** The study sites are particularly suitable for aeolian processes, except in cases of episodic storms, because the backshore is almost always above the recurrent sea level position. This situation allows the beach to remain dry and is very favourable for wind sediment transport (Cooper, 1994; Sabatier et al., 2007, 2004). This is particularly important in the study area, where the offshore wind is dominant (73% of the time) which can allow, depending on the sediment availability, a scouring of the emerged beach that can reach -0.3 m and a shoreline advance over several metres (**Fig.7**). Thus, on an annual scale, the emerged beach is not only affected by onshore sediment transport and superficial deposits during marine storm events but also by offshore sediment transport during offshore wind events. During which, some of this sediment is redistributed onto the beach and foreshore by the

offshore wind (Dingler et al., 1992; Gares et al., 1996; Jackson and Nordstrom, 1997; Leatherman, 1979; Nordstrom et al., 1996; Sabatier et al., 2007, 2004). The opposition of onshore and offshore forcing agents highlights the particular balance of sediment transport between the backshore/dune system and the shoreline (Dingler et al., 1992; Leatherman, 1979; Sabatier et al., 2007; Wright et al., 1985). However, the specific effect of offshore wind on the dynamics of the emerged beach and its sediment budget is sparsely addressed in the literature and deserve to be studied in more detail given its importance at certain locations.

6. Conclusion

Surveys were carried out on the beaches of Leucate and La Franqui over a period of 4 years; both sites are characterised by dominant offshore winds, contrasting wave regimes and low microtidal range. These forcing conditions lead to the development of a model with five situations driven by a strong seasonality describing the emerged beach response. This model can be applied to most of the southern sandy coastline of the Gulf of Lions (45 km of coast) and more generally, the dynamics described here may possibly concern some beaches of the Mediterranean and other closed seas. The offshore wind, due to its transport capacity and predominance (73% of the time), can have an erosive action up to - 0.3 m on the top of the backshore (situation 1). The consequent transport of sand to the coastline leads to an accretion on the beach face (up to + 0.4 m) which generates a uniform advance of the coastline (of up to several metres). The action of low-intensity waves ($Hs < 1$ m), either combined with offshore wind and sediment transport from the backshore to the coastline (situation 2) or associated with a stable backshore, without offshore wind forcing (situation 3), leads to accretion and advance of the megacusps horns due to wave refraction on the horns accompanied by a slight erosion and potential retreat of the embayments. The morphogenetic impacts of these fair-weather conditions are clearly visible, notably at the foot of the beach face, due to the constant sea level position over time characteristic of this low-microtidal environment. More dynamic onshore wave conditions ($Hs > 1$ m and higher) either without wind or only with onshore winds, lead to erosion of the lower beach by wave attack paired with a large swash creating a higher berm with a steeper beach face in a retreated position (situation 4). Following the short but violent storm episodes that occur in the Mediterranean (situation 5), the retreat of the berm is maximal and can become established on the central part of the pre-storm beach. This can also result in sediment deposition on the upper beach along the dune toe or in the form of washover deposits. The construction of this

massive sedimentary feature, not necessarily observed for high microtidal regimes and then stable during months until the next storm, is possible because of the relatively stable and high water level during the storm event permitting thus the construction of the berm during all the storm duration. The alternation of storm episodes and offshore wind periods could control the relative stability of the emerged beach.

Acknowledgements

The authors would like to thank the Region Occitanie for the grant thesis support, ObsCat, the PNM du Golfe du Lion and the PNR de la Narbonnaise en Méditerranée for their financial support. Leucate is a monitoring site of Service National d'Observation (SNO) Dynalit. Dr M.S.N. Carpenter post-edited the English style and grammar.

Literature cited

Aagaard, T., Kroon, A., Andersen, S., Møller Sørensen, R., Quartel, S., Vinther, N., 2005. Intertidal beach change during storm conditions; Egmond, The Netherlands. Marine Geology 218, 65–80. https://doi.org/10.1016/j.margeo.2005.04.001

Aleman, N., Robin, N., Certain, R., Anthony, E.J., Barusseau, J.P., 2015. Longshore variability of beach states and bar types in a microtidal, storm-influenced, low-energy environment. Geomorphology 241, 175–191. https://doi.org/10.1016/j.geomorph.2015.03.029

Aleman, N., Robin, N., Certain, R., Vanroye, C., Barusseau, J.P., Bouchette, F., 2011. Typology of nearshore bars in the Gulf of Lions (France) using LIDAR technology. Journal of Coastal Research 721–725.

Amores, A., Marcos, M., Carrió Carrió, D., Gómez-Pujol, L., 2020. Coastal Impacts of Storm Gloria (January 2020) over the Northwestern Mediterranean. https://doi.org/10.5194/nhess-2020-75

Armaroli, C., Ciavola, P., Perini, L., Calabrese, L., Lorito, S., Valentini, A., Masina, M., 2012. Critical storm thresholds for significant morphological changes and damage along the Emilia-Romagna coastline, Italy. Geomorphology 143. https://doi.org/10.1016/j.geomorph.2011.09.006

Armaroli, C., Grottoli, E., Harley, M.D., Ciavola, P., 2013. Beach morphodynamics and types of foredune erosion generated by storms along the Emilia-Romagna coastline, Italy. Geomorphology, COASTAL GEOMORPHOLOGY AND RESTORATION 44TH BINGHAMTON GEOMORPHOLOGY SYMPOSIUM 199, 22–35. https://doi.org/10.1016/j.geomorph.2013.04.034

Balouin, Y., Ciavola, P., Armaroli, C., 2005. Sediment Transport Pattern and Coastal Evolution at Lido di Dante Beach, Adriatic Sea, Coastal Dynamics 2005 - Proceedings of the Fifth Coastal Dynamics International Conference. https://doi.org/10.1061/40855(214)65

Balouin, Y., Tesson, J., Gervais, M., 2013. Cuspate shoreline relationship with nearshore bar dynamics during storm events – field observations at Sete beach, France. Journal of Coastal Research 65, 440–445. https://doi.org/10.2112/SI65-075.1

636 Bauer, B.O., Davidson-Arnott, R.G.D., Walker, I.J., Hesp, P.A., Ollerhead, J., 2012. Wind
637 direction and complex sediment transport response across a beach–dune system. Earth
638 Surface Processes and Landforms 37, 1661–1677. https://doi.org/10.1002/esp.3306
639 Benavente, J., Harris, D., Austin, T.P., Vila-Concejo, A., 2011. Medium term behavior and
640 evolution of a beach cusps system in a low energy beach, Port Stephens, NSW,
641 Australia. Journal of Coastal Research SI, 170–174.
642 Bertoni, D., Grottoli, E., Ciavola, P., Sarti, G., Benelli, G., Pozzebon, A., 2013. On the
643 displacement of marked pebbles on two coarse-clastic beaches during short fair-
644 weather periods (Marina di Pisa and Portonovo, Italy). Geo-Mar Lett 33, 463–476.
645 https://doi.org/10.1007/s00367-013-0341-3
646 Birrien, F., Castelle, B., Dailloux, D., Marieu, V., Rihouey, D., Price, T., 2013. Video
647 observation of megacusp evolution along a high-energy engineered sandy beach:
648 Anglet, SW France. coas 65, 1727–1732. https://doi.org/10.2112/SI65-292.1
649 Bugajny, N., Furmańczyk, K., 2020. Short-term Volumetric Changes of Berm and Beachface
650 during Storm Calming. coas 95, 398–402. https://doi.org/10.2112/SI95-077.1
651 Buosi, C., Ibba, A., Passarella, M., Porta, M., Ruju, A., Trogu, D., De Muro, S., 2019.
652 Geomorphology, beach classification and seasonal morphodynamic transition of a
653 Mediterranean gravel beach (Sardinia, Gulf of Cagliari). Journal of Maps 15, 165–
654 176. https://doi.org/10.1080/17445647.2019.1567402
655 Casamayor, M., Alonso, I., Valiente, N.G., Sánchez-García, M.J., 2022. Seasonal response of
656 a composite beach in relation to wave climate. Geomorphology 108245.
657 https://doi.org/10.1016/j.geomorph.2022.108245
658 Castelle, B., Bonneton, P., Dupuis, H., Sénéchal, N., 2007. Double bar beach dynamics on
659 the high-energy meso-macrotidal French Aquitanian Coast: A review. Marine
660 Geology 245, 141–159. https://doi.org/10.1016/j.margeo.2007.06.001
661 Castelle, B., Marieu, V., Bujan, S., 2019. Alongshore-Variable Beach and Dune Changes on
662 the Timescales from Days (Storms) to Decades Along the Rip-dominated Beaches of
663 the Gironde Coast, SW France. Journal of Coastal Research 88, 157–171.
664 https://doi.org/10.2112/SI88-012.1
665 Castelle, B., Marieu, V., Bujan, S., Splinter, K.D., Robinet, A., Sénéchal, N., Ferreira, S.,
666 2015. Impact of the winter 2013–2014 series of severe Western Europe storms on a
667 double-barred sandy coast: Beach and dune erosion and megacusp embayments.
668 Geomorphology 238, 135–148. https://doi.org/10.1016/j.geomorph.2015.03.006
669 Cerema, C. d'étude et d'expertise sur les risques, l'environnement, la mobilité et
670 l'aménagement, Dreal LR, Observatoire Océanologique de Banyuls, 2019. CANDHIS
671 - Détail de la campagne 01101 - Leucate [WWW Document]. Centre d'Archivage
672 National de Données de Houle In Situ. URL http://candhis.cetmef.developpement-
673 durable.gouv.fr/campagne/?idcampagne=c81e728d9d4c2f636f067f89cc14862c
674 (accessed 4.1.19).
675 Cerema, Dreal LR, 2018. Fiche synthétique de la campagne 01001 Leucate.
676 Certain, R., 2002. Morphodynamique d'une côte sableuse microtidale à barres: le Golfe du
677 Lion (Languedoc-Roussillon) (Thèse). Université de Perpignan, Perpignan.
678 Coco, G., Huntley, D.A., O'Hare, T.J., 2000. Investigation of a self-organization model for
679 beach cusp formation and development. Journal of Geophysical Research: Oceans
680 105, 21991–22002. https://doi.org/10.1029/2000JC900095
681 Cooper, J.A.G., 1994. Lagoons and microtidal coasts, in: Carter, R.W.G., Woodroffe, C.D.
682 (Eds.), Coastal Evolution Late Quaternary Shoreline Morphodynamics. pp. 219–265.
683 Costas, S., Alejo, I., Vila-Concejo, A., Nombela, M., 2005. Persistence of storm-induced
684 morphology on a modal low-energy beach: A case study from NW-Iberian Peninsula.
685 Marine Geology 43–56. https://doi.org/10.1016/j.margeo.2005.08.003

686 Davidson, M.A., Splinter, K.D., Turner, I.L., 2013. A simple equilibrium model for
687 predicting shoreline change. Coastal Engineering 73, 191–202.
688 https://doi.org/10.1016/j.coastaleng.2012.11.002
689 Davidson, M.A., Turner, I.L., Splinter, K.D., Harley, M.D., 2017. Annual prediction of
690 shoreline erosion and subsequent recovery. Coastal Engineering 130, 14–25.
691 https://doi.org/10.1016/j.coastaleng.2017.09.008
692 Davidson-Arnott, R.G.D., Yang, Y., Ollerhead, J., Hesp, P.A., Walker, I.J., 2008. The effects
693 of surface moisture on aeolian sediment transport threshold and mass flux on a beach.
694 Earth Surface Processes and Landforms 33, 55–74. https://doi.org/10.1002/esp.1527
695 De Muro, S., Pusceddu, N., Buosi, C., Ibba, A., 2017. Morphodynamics of a Mediterranean
696 microtidal wave-dominated beach: forms, processes and insights for coastal
697 management. Journal of Maps 13, 26–36.
698 https://doi.org/10.1080/17445647.2016.1250681
699 de Swart, R., Ribas, F., Calvete, D., Simarro, G., Guillen, J., 2022. Observations of megacusp
700 dynamics and their coupling with crescentic bars at an open, fetch-limited beach.
701 Earth Surface Processes and Landforms. https://doi.org/10.1002/esp.5451
702 Delgado-Fernandez, I., Jackson, D., Cooper, A., Baas, A., Beyers, M., 2013. Field
703 characterization of three-dimensional lee-side airflow patterns under offshore winds at
704 a beach-dune system. Journal of Geophysical Research: Earth Surface 118, 706–721.
705 https://doi.org/10.1002/jgrf.20036
706 Dingler, J.R., Hsu, S.A., Reiss, T.E., 1992. Theoretical and measured aeolian sand transport
707 on a barrier island, Louisiana, USA. Sedimentology 39, 1031–1043.
708 https://doi.org/10.1111/j.1365-3091.1992.tb01995.x
709 Dolique, F., Sedrati, M., Charpentier, J., Jeanson, M., Cohen, O., Dupuy, L., Alami, S., 2019.
710 Beaches Seasonal and Paroxysmal Morphosedimentary Dynamics: Results of 10
711 years Martinique Coastal Observation Network. Journal of Coastal Research 88, 172–
712 184. https://doi.org/10.2112/SI88-013.1
713 Durán, R., Guillén, J., Ruiz, A., Jiménez, J.A., Sagristà, E., 2016. Morphological changes,
714 beach inundation and overwash caused by an extreme storm on a low-lying embayed
715 beach bounded by a dune system (NW Mediterranean). Geomorphology 274, 129–
716 142. https://doi.org/10.1016/j.geomorph.2016.09.012
717 Eichentopf, S., Alsina, J.M., Christou, M., Kuriyama, Y., Karunarathna, H., 2020. Storm
718 sequencing and beach profile variability at Hasaki, Japan. Marine Geology 106153.
719 https://doi.org/10.1016/j.margeo.2020.106153
720 Eichentopf, S., Karunarathna, H., Alsina, J.M., 2019a. Morphodynamics of sandy beaches
721 under the influence of storm sequences: Current research status and future needs.
722 Water Science and Engineering 12, 221–234.
723 https://doi.org/10.1016/j.wse.2019.09.007
724 Eichentopf, S., van der Zanden, J., Cáceres, I., Alsina, J.M., 2019b. Beach Profile Evolution
725 towards Equilibrium from Varying Initial Morphologies. JMSE 7, 406.
726 https://doi.org/10.3390/jmse7110406
727 Falqués, A., Ribas, F., Mujal-Colilles, A., Puig-Polo, C., 2021. A New Morphodynamic
728 Instability Associated With Cross-Shore Transport in the Nearshore. Geophysical
729 Research Letters 48, e2020GL091722. https://doi.org/10.1029/2020GL091722
730 Fanini, L., Defeo, O., Elliott, M., 2020. Advances in sandy beach research – Local and global
731 perspectives. Estuarine, Coastal and Shelf Science 234, 106646.
732 https://doi.org/10.1016/j.ecss.2020.106646
733 Ferrer, P., 2010. Morphodynamique à multi-échelles du trait de côte (prisme sableux) du
734 golfe du Lion depuis le dernier optimum climatique (Thèse). Université de Perpignan
735 Via Domitia, Perpignan.

Feyssat, P., Certain, R., Robin, N., Raynal, O., Aleman, N., Hebert, B., Lamy, A., Barusseau, J.-P., 2022. Morphodynamic Behaviour of a Mediterranean Intermittent Estuary with Opening Phases Primarily Dominated by Offshore Winds. Journal of Marine Science and Engineering 10, 1817. https://doi.org/10.3390/jmse10121817

Gallop, S.L., Bryan, K.R., Coco, G., Stephens, S.A., 2011. Storm-driven changes in rip channel patterns on an embayed beach. Geomorphology 127, 179–188. https://doi.org/10.1016/j.geomorph.2010.12.014

Gares, P.A., Davidson-Arnott, R.G.D., Bauer, B.O., Sherman', D.J., Carter, R.W.G., Jackson', D.W.T., Nordstromt, K.F., 1996. Aeolian Sediment Transport Under Offshore Wind Conditions: Implications for Aeolian Sediment Budget Calculations. Journal of Coastal Research 673–682.

Gervais, M., 2012. Impacts morphologiques des surcotes et vagues de tempêtes sur le littoral méditerranéen. Université de Perpignan.

Gervais, M., Balouin, Y., Belon, R., 2012a. Morphological response and coastal dynamics associated with major storm events along the Gulf of Lions Coastline, France. Geomorphology, Thresholds for storm impacts along European coastlines 143–144, 69–80. https://doi.org/10.1016/j.geomorph.2011.07.035

Gervais, M., Balouin, Y., Belon, R., 2012b. Morphological response and coastal dynamics associated with major storm events along the Gulf of Lions Coastline, France. Geomorphology 143–144, 69–80. https://doi.org/10.1016/j.geomorph.2011.07.035

Gervais, M., Balouin, Y., Belon, R., Certain, R., Robin, N., Berne, S., 2010. Impacts des tempêtes sur la morphologie d'un littoral microtidal : le site du Lido de Sète à Marseillan, Golfe du Lion, in: XIèmes Journées, Les Sables d'Olonne. Presented at the Journées Nationales Génie Côtier - Génie Civil, Editions Paralia, pp. 263–274. https://doi.org/10.5150/jngcgc.2010.032-G

Gómez-Pujol, L., Orfila, A., Álvarez-Ellacuría, A., Tintoré, J., 2011. Controls on sediment dynamics and medium-term morphological change in a barred microtidal beach (Cala Millor, Mallorca, Western Mediterranean). Geomorphology 132, 87–98.

Gómez-Pujol, L., Orfila, A., Cañellas, B., Alvarez-Ellacuria, A., Méndez, F.J., Medina, R., Tintoré, J., 2007. Morphodynamic classification of sandy beaches in low energetic marine environment. Marine Geology 242, 235–246. https://doi.org/10.1016/j.margeo.2007.03.008

Guizien, K., 2009. Spatial variability of wave conditions in the Gulf of Lions (NW-Mediterranean Sea). Life and Environment 59, 261–270.

Guza, R., Inman, D., 1975. Edge waves and beach cusps. Journal of Geophysical Research 80, 2997–3012. https://doi.org/10.1029/JC080i021p02997

He, Y., Liu, J., Cai, F., Li, B., Qi, H., Zhao, S., 2022. Aeolian sand transport influenced by tide and beachface morphology. Geomorphology 396, 107987. https://doi.org/10.1016/j.geomorph.2021.107987

Hegge, B., Eliot, I., Hsu, J., 1996. Sheltered Sandy Beaches of Southwestern Australia. Journal of Coastal Research 12, 748–760.

Itzkin, M., Moore, L.J., Ruggiero, P., Hacker, S.D., 2020. The effect of sand fencing on the morphology of natural dune systems. Geomorphology 352, 106995. https://doi.org/10.1016/j.geomorph.2019.106995

Jackson, D., Beyers, M., Delgado-Fernandez, I., Baas, A., Cooper, A., 2013. Airflow reversal and alternating corkscrew vortices in foredune wake zones during perpendicular and oblique offshore winds. Geomorphology 187, 86–93. https://doi.org/10.1016/j.geomorph.2012.12.037

Jackson, N.L., Nordstrom, K.F., 1997. Effects of Time-dependent Moisture Content of Surface Sediments on Aeolian Transport Rates Across a Beach, Wildwood, New

Jersey, U.S.A. Earth Surface Processes and Landforms 22, 611–621. https://doi.org/10.1002/(SICI)1096-9837(199707)22:7<611::AID-ESP715>3.0.CO;2-1

Jackson, N.L., Nordstrom, K.F., Eliot, I., Masselink, G., 2002. 'Low energy' sandy beaches in marine and estuarine environments: a review. Geomorphology, 29th Binghamton Geomorphology Symposium: Coastal Geomorphology 48, 147–162. https://doi.org/10.1016/S0169-555X(02)00179-4

Käärd, A., Valdmann, A., Eelsalu, M., Pindsoo, K., Männikus, R., Soomere, T., 2016. Preventive management of undesired changes in alongshore sediment transport in the planning of a waterfront infrastructure. https://doi.org/10.2495/SC160361

Karunarathna, H., Pender, D., Ranasinghe, R., Short, A.D., Reeve, D.E., 2014. The effects of storm clustering on beach profile variability. Marine Geology 348, 103–112. https://doi.org/10.1016/j.margeo.2013.12.007

Kennedy, D.M., McSweeney, S.L., Mariani, M., Zavadil, E., 2020. The geomorphology and evolution of intermittently open and closed estuaries in large embayments in Victoria, Australia. Geomorphology 350, 106892. https://doi.org/10.1016/j.geomorph.2019.106892

Konstantinou, A., Stokes, C., Masselink, G., Scott, T., 2021. The extreme 2013/14 winter storms: Regional patterns in multi-annual beach recovery. Geomorphology 107828. https://doi.org/10.1016/j.geomorph.2021.107828

Kulling, B., 2017. Déformation du rivage et dérive littorale des plages du Golfe du Lion (Thèse). Université d'Aix-Marseille.

Law, M.N., Davidson-Arnott, R., 1990a. Seasonal controls on aeolian processes on the beach and foredune. Proceedings of Symposium on Coastal Sand Dunes 49–68.

Law, M.N., Davidson-Arnott, R., 1990b. Seasonal controls on aeolian processes on the beach and foredune. Proceedings of Symposium on Coastal Sand Dunes 49–68.

Leatherman, S., 1979. Barrier dune systems: a reasssessment.

Li, L., Barry, D., Parlange, J.-Y., Pattiaratchi, C., 1997. Beach water table fluctuations due to wave run-up: Capillarity effects. Water Resources Research 33. https://doi.org/10.1029/96WR03946

Lippmann, T.C., Holman, R.A., 1990. The spatial and temporal variability of sand bar morphology. J. Geophys. Res. 95, 11575. https://doi.org/10.1029/JC095iC07p11575

Longhitano, S.G., 2015. Short-Term Assessment of Retreating vs. Advancing Microtidal Beaches Based on the Backshore/Foreshore Length Ratio: Examples from the Basilicata Coasts (Southern Italy). OJMS 05, 123–145. https://doi.org/10.4236/ojms.2015.51011

Lynch, K., Delgado-Fernandez, I., Jackson, D.W.T., Cooper, J.A.G., Baas, A.C.W., Beyers, J.H.M., 2013. Alongshore variation of aeolian sediment transport on a beach, under offshore winds. Aeolian Research 8, 11–18. https://doi.org/10.1016/j.aeolia.2012.10.004

Masselink, G., Pattiaratchi, C.B., 2001. Seasonal changes in beach morphology along the sheltered coastline of Perth, Western Australia. Marine Geology 172, 243–263. https://doi.org/10.1016/S0025-3227(00)00128-6

Masselink, G., Short, A., 1993. The effect of tide range on beach morphodynamics and morphology: a conceptual beach model. Journal of Coastal Research 9, 785–800.

McSweeney, Stout, J.C., Kennedy, D.M., 2020. Variability in infragravity wave processes during estuary artificial entrance openings. Earth Surface Processes and Landforms 45, 3414–3428. https://doi.org/10.1002/esp.4974

834 Medellín, G., Torres-Freyermuth, A., 2021. Foredune formation and evolution on a
835 prograding sea-breeze dominated beach. Continental Shelf Research 226, 104495.
836 https://doi.org/10.1016/j.csr.2021.104495
837 Mendoza, E., Jiménez, J., 2006. Storm-Induced Beach Erosion Potential on the Catalonian
838 Coast. Journal of Coastal Research SI 48, 81–88.
839 Mendoza, E., Jiménez, J., Mateo, J., 2011. A coastal storms intensity scale for the Catalan sea
840 (NW Mediterranean). Natural Hazards and Earth System Sciences - NAT HAZARDS
841 EARTH SYST SCI 11, 2453–2462. https://doi.org/10.5194/nhess-11-2453-2011
842 Meslard, F., Balouin, Y., Robin, N., Bourrin, F., 2022. Assessing the Role of Extreme
843 Mediterranean Events on Coastal River Outlet Dynamics. Water 14, 2463.
844 https://doi.org/10.3390/w14162463
845 Namikas, S.L., Edwards, B.L., Bitton, M.C.A., Booth, J.L., Zhu, Y., 2010. Temporal and
846 spatial variabilities in the surface moisture content of a fine-grained beach.
847 Geomorphology 114, 303–310. https://doi.org/10.1016/j.geomorph.2009.07.011
848 Nordstrom, K.F., 2021. Developed Coasts, in: Reference Module in Earth Systems and
849 Environmental Sciences. Elsevier. https://doi.org/10.1016/B978-0-12-818234-
850 5.00056-0
851 Nordstrom, K.F., Bauer, B.O., Davidson-Arnott, R.G.D., Garesc, P.A., Carter, R.W.G.,
852 Jackson', D.W.T., Sherman', D.J., 1996. Offshore Aeolian Transport Across a Beach:
853 Carrick Finn Strand, Ireland. Journal of Coastal Research 664–672.
854 Nordstrom, K.F., Jackson, N.L., 2017. Offshore aeolian sediment transport across a human-
855 modified foredune. Earth Surf. Process. Landforms 43, 195–201.
856 https://doi.org/10.1002/esp.4217
857 Phillips, M.S., Harley, M.D., Turner, I.L., Splinter, K.D., Cox, R.J., 2017. Shoreline recovery
858 on wave-dominated sandy coastlines: the role of sandbar morphodynamics and
859 nearshore wave parameters. Marine Geology 385, 146–159.
860 https://doi.org/10.1016/j.margeo.2017.01.005
861 Porta, M., Buosi, C., Trogu, D., Ibba, A., Muro, S., 2020. An integrated sea-land approach for
862 analyzing forms, processes, deposits and the evolution of the urban coastal belt of
863 Cagliari. Journal of Maps 17, 1–10. https://doi.org/10.1080/17445647.2020.1719441
864 Power, H.E., Pomeroy, A.W.M., Kinsela, M.A., Murray, T.P., 2021. Research Priorities for
865 Coastal Geoscience and Engineering: A Collaborative Exercise in Priority Setting
866 From Australia. Frontiers in Marine Science 8, 252.
867 https://doi.org/10.3389/fmars.2021.645797
868 Quartel, S., 2009. Temporal and spatial behaviour of rip channels in a multiple-barred coastal
869 system. Earth Surface Processes and Landforms 34, 163–176.
870 https://doi.org/10.1002/esp.1685
871 Quartel, S., Kroon, A., Ruessink, B.G., 2008. Seasonal accretion and erosion patterns of a
872 microtidal sandy beach. Marine Geology 250, 19–33.
873 https://doi.org/10.1016/j.margeo.2007.11.003
874 Robin, N., Billy, J., Castelle, B., Hesp, P., Nicolae Lerma, A., Laporte-Fauret, Q., Marieu, V.,
875 Rosebery, D., Bujan, S., Destribats, B., Michalet, R., 2020. 150 years of foredune
876 initiation and evolution driven by human and natural processes. Geomorphology,
877 sediment 374, 107516. https://doi.org/10.1016/j.geomorph.2020.107516
878 Romagnoli, C., Sistilli, F., Cantelli, L., Aguzzi, M., Nigris, N., Morelli, M., Gaeta, M.,
879 Archetti, R., 2021. Beach Monitoring and Morphological Response in the Presence of
880 Coastal Defense Strategies at Riccione (Italy). Journal of Marine Science and
881 Engineering 9, 851. https://doi.org/10.3390/jmse9080851
882 Ruiz de Alegría-Arzaburu, A., Gracia-Barrera, A.D., Kono-Martínez, T., Coco, G., 2022.
883 Subaerial and upper-shoreface morphodynamics of a highly-dynamic enclosed beach

884 in NW Baja California. Geomorphology 413, 108336.
885 https://doi.org/10.1016/j.geomorph.2022.108336
886 Sabatier, F., Chaïbi, M., Chauvelon, P., 2007. Transport éolien par vent de mer et
887 alimentation sédimentaire des dunes de Camargue. mediterranee 83–90.
888 https://doi.org/10.4000/mediterranee.177
889 Sabatier, F., Heurtefeux, H., Hanot, B., 2008. Dépôts d'overwash et tempêtes à moyen terme
890 sur deux lidos méditerranéens, in: Xèmes Journées, Sophia Antipolis. Presented at the
891 Journées Nationales Génie Côtier - Génie Civil, Editions Paralia, pp. 477–486.
892 https://doi.org/10.5150/jngcgc.2008.046-S
893 Sabatier, F., Samat, O., Chaibi, M., Lambert, A., Pons, F., 2004. Transport sédimentaire de la
894 dune à la zone du déferlement sur une plage sableuse soumise à des vents de terre, in:
895 VIIIèmes Journées Nationales Génie Civil – Génie Côtier. Compiègne.
896 Sallenger, A.H., 2000. Storm Impact Scale for Barrier Islands. Journal of Coastal Research
897 16, 890–895.
898 Schwarz, C., Starrenburg, C. van, Donker, J., Ruessink, G., 2021. Wind and Sand Transport
899 Across a Vegetated Foredune Slope. Journal of Geophysical Research: Earth Surface
900 126, e2020JF005732. https://doi.org/10.1029/2020JF005732
901 Scott, T., Masselink, G., Russell, P., 2011. Morphodynamic characteristics and classification
902 of beaches in England and Wales. Marine Geology 286, 1–20.
903 Sedrati, M., Ciavola, P., Armaroli, C., 2011. Morphodynamic evolution of a microtidal
904 barrier, the role of overwash: Bevano, Northern Adriatic Sea. Journal of Coastal
905 Research.
906 Sedrati, M., Ciavola, P., Reyns, J., Armaroli, C., Sipka, V., 2009. Morphodynamics of a
907 Microtidal Protected Beach During Low Wave-energy Conditions. Journal of Coastal
908 Research 198–202.
909 Segura, L.E., Hansen, J.E., Lowe, R.J., Symonds, G., Contardo, S., 2018. Shoreline
910 variability at a low-energy beach: Contributions of storms, megacusps and sea-breeze
911 cycles. Marine Geology 400, 94–106. https://doi.org/10.1016/j.margeo.2018.03.008
912 Senechal, N., Ruiz de Alegria-Arzaburu, A., 2020. 20 - Seasonal imprint on beach
913 morphodynamics, in: Jackson, D.W.T., Short, A.D. (Eds.), Sandy Beach
914 Morphodynamics. Elsevier, pp. 461–486. https://doi.org/10.1016/B978-0-08-102927-
915 5.00020-5
916 Short, A., Woodroffe, C., 2009. The coast of Australia. Faculty of Science - Papers (Archive)
917 300.
918 Short, A.D., Aagaard, T., 2020. Single and Multi-Bar Beach Change Models. Journal of
919 Coastal Research 18.
920 Short, A.D., Hesp, P.A., 1982. Wave, beach and dune interactions in southeastern Australia.
921 Marine Geology 48, 259–284. https://doi.org/10.1016/0025-3227(82)90100-1
922 Soomere, T., Pindsoo, K., Kudryavtseva, N., Eelsalu, M., 2020. Variability of distributions of
923 wave set-up heights along a shoreline with complicated geometry. Ocean Science 16,
924 1047–1065. https://doi.org/10.5194/os-16-1047-2020
925 Stockdon, H.F., Holman, R.A., Howd, P.A., Sallenger, A.H., 2006. Empirical
926 parameterization of setup, swash, and runup. Coastal Engineering 53, 573–588.
927 https://doi.org/10.1016/j.coastaleng.2005.12.005
928 Thornton, E.B., MacMahan, J., Sallenger, A.H., 2007. Rip currents, mega-cusps, and eroding
929 dunes. Marine Geology 240, 151–167. https://doi.org/10.1016/j.margeo.2007.02.018
930 Trogu, D., Buosi, C., Ruju, A., Porta, M., Ibba, A., De Muro, S., 2020. What Happens to a
931 Mediterranean Microtidal Wave-dominated Beach During Significant Storm Events?
932 The Morphological Response of a Natural Sardinian Beach (Western Mediterranean).
933 Journal of Coastal Research 95, 695–700. https://doi.org/10.2112/SI95-135.1

Van Gaalen, J.F., Kruse, S.E., Coco, G., Collins, L., Doering, T., 2011. Observations of beach cusp evolution at Melbourne Beach, Florida, USA. Geomorphology 129, 131–140. https://doi.org/10.1016/j.geomorph.2011.01.019

Walker, I.J., Hesp, P.A., Smyth, T.A.G., 2022. 7.16 - Airflow Dynamics Over Unvegetated and Vegetated Dunes, in: Shroder, J. (Jack) F. (Ed.), Treatise on Geomorphology (Second Edition). Academic Press, Oxford, pp. 415–453. https://doi.org/10.1016/B978-0-12-818234-5.00136-X

Walker, I.J., Shugar, D.H., 2013. Secondary flow deflection in the lee of transverse dunes with implications for dune morphodynamics and migration. Earth Surf. Process. Landforms 38, 1642–1654. https://doi.org/10.1002/esp.3398

Wright, L.D., Short, A.D., 1984. Morphodynamic variability of surf zones and beaches: A synthesis. Marine Geology 56, 93–118. https://doi.org/10.1016/0025-3227(84)90008-2

Wright, L.D., Short, A.D., Green, M.O., 1985. Short-term changes in the morphodynamic states of beaches and surf zones: An empirical predictive model. Marine Geology 62, 339–364. https://doi.org/10.1016/0025-3227(85)90123-9

Yates, M.L., Guza, R.T., O'Reilly, W.C., 2009. Equilibrium shoreline response: Observations and modeling. Journal of Geophysical Research: Oceans 114. https://doi.org/10.1029/2009JC005359